IEEE Access
Multidisciplinary | Rapid Review | Open Access Journal

Received February 17, 2020, accepted March 1, 2020, date of current version March 18, 2020.

Digital Object Identifier 10.1109/ACCESS.2020.2978621

Computation of Power Extraction From Photovoltaic Arrays Under Various Fault Conditions

AZHAR UL-HAQ[1], RASHID ALAMMARI[2], ATIF IQBAL[2], (Senior Member, IEEE), MARIUM JALAL[3,4], AND SABA GUL[1]

[1]Department of Electrical Engineering, NUST College of EME, National University of Sciences and Technology (NUST), Islamabad, 46000 Pakistan
[2]Department of Electrical Engineering, College of Engineering, Qatar University, Doha, Qatar
[3]Department of Electronic Engineering, Fatima Jinnah Women University, Rawalpindi, 46000 Pakistan
[4]Department of Electrical Engineering, Lahore College for Women University, Lahore, 54000 Pakistan

Corresponding author: Rashid Alammari (ralammari@qu.edu.qa)

The research work is supported by Qatar University under its National Capacity Building Project (NCBP) Research Grant.

ABSTRACT Photovoltaic (PV) faults such as partial shading, bypass-diode defects, degradation of PV modules, and wiring issues greatly affect the power output and cause various peaks in P-V curves of a PV system. Although, commonly used Total-Cross-Tied (TCT) scheme in PV arrays is considered instrumental for reducing power losses there lies a great scope to evaluate power extraction through reconfiguration of modules with different PV materials. This paper presents detailed investigation of power extraction using number placement reconfiguration method under numerous faults. PV power extraction is carried out and compared with three different interconnections of PV modules, including series-parallel (SP), bridge-link (BL) and TCT. In order to conduct a thorough investigation and better evaluate the performance of PV arrays, we have studied reconfiguration of PV modules with polycrystalline and copper indium gallium selenide (CIGS) PV technologies. In addition, this paper contains detailed quantification of the impact of the studied PV faults on power grid. The results obtained in MATLAB/Simulink demonstrate that CIGS PV technology performs better than polycrystalline in terms of power output during different faulty conditions. It becomes evident from the presented results that optimal reconfiguration of PV arrays can increase the power extraction from PV system with reduced number of P-V peaks. Hence, leading to improved performance of the PV system.

INDEX TERMS PV system, PV fault analysis, reconfiguration method, PV technologies, power grid.

I. INTRODUCTION

Significant rise in the advancement of photovoltaic (PV) technology has been witnessed worldwide during the recent years despite its high susceptibility to numerous faults such as partial shading, wiring losses, disconnection of PV modules, defects in bypass diodes and hot spot heating [1]–[3]. All such faults can cause multiple peaks in P-V characteristic curve leading to degraded performance of the PV arrays [4].

Many studies have been conducted to quantify the impact of partial shading on PV system's output power and power losses [5]–[9]. Authors in [10], [11], studied the impact of shading on two different PV technologies including thin film and crystalline. The previous research shows that crystalline PV technology has less tolerance towards shading conditions and can cause significant power losses due to the former's low efficiency [12]. Nonetheless, there is a great opportunity to investigate different approaches for improving fault tolerance and to extract maximum power from PV arrays under different faulty conditions. Authors in [13]–[17] adopted static topologies with reconfigurations algorithms to optimize power generation from PV arrays under non-uniform shading. A comprehensive reconfiguration algorithm is presented in [18], [19] to increase peak power but the given methodology requires many sensors, employs complex switching matrix for a relatively small PV array, which not only make the control circuitry and design complicated to implement but also increases the cost. Most of such reconfiguration algorithms investigate the faults' impact for only shading conditions. Thus, further research is needed to investigate

The associate editor coordinating the review of this manuscript and approving it for publication was Anisul Haque.

TABLE 1. Literature review with identification of research gaps.

Sr. No	Technique for fault analysis	Research Gaps	Ref.
1	Dominance square and competence square method under shading patterns	Physical relocation needed. Only shading is analyzed	[20-22]
2	Electrical array reconfiguration using matrix switching	Implemented on a small array. Complex switching matrix with many sensors	[23]
3	Dynamic part of array is balanced with static part for equalizing shading	Complex switching for balancing the shade	[24]
4	Different irradiance with reconfiguration through removal of shaded modules	Removal of shaded modules create un balanced voltage level	[25]
5	Shading analysis using image processing	Shading analyzed only for small array	[26]
6	SuDoKu method for analyzing shading fault	Needs physical relocation Wire losses due to increase in wire length Depends on shading dispersion factor	[27]
7	Genetic algorithm for reconfiguration	Only for even rows and column	[28,29]
8	Particle swarm optimization for reconfiguration	Only for even no. of rows and columns	[30]
9	Optimal SuDoKu method to enhance power under shading	Optimization of SuDoKu decreases power losses but the effectiveness of technique is only proved for the defined shading patterns	[31]
10	Shading dispersion (SD) physical array relocation (PAR) technique for maximum power generation for partially shaded PV arrays	Only for row shading Implemented on a small 3×3 PV array	[32]

suitable methods for maximum power extraction under above mentioned fault scenarios through optimal placement of PV modules. A number placement method has been employed in the literature for analyzing the impact of shading with different topologies, [20]–[22].

Authors in [22] have applied competence square (CS) method for power maximization from PV arrays through physical relocation of PV modules. PV module reconfiguration through physical relocation has gained attention in the recent years due to its less cost and relatively simple circuit-rythan reconfiguration through complex switching matrix. Different shade dispersion techniques have been investigated in literature like optimal TCT, Sudoku and optimal Sudoku to address partial shading faults [23]–[32]. All those techniques have been mainly aimed to minimize the shading impact through defining specific number pattern. It was established that partial shading can be minimized by sudoku method at the cost of increased wiring losses. Author in [31] have used optimal sudoku method to decrease shading losses through overcoming the demerits of simple sudoku method but its analysis is limited to specific shading patterns. Shading dispersion (SD) physical array relocation (PAR) technique for maximum power extraction has been reported in [32] for partially shaded PV arrays but this technique reduces row shading through removing shaded modules in a row. Detailed literature review with identified research gaps is presented in Table 1.

In this research paper, a reconfiguration method (RM) of number placement is applied through altering the position of PV modules without changing the adopted interconnections of PV modules. The presented relocation method is used for maximizing the generated peak power (PP) under various fault scenarios. The relocation method is compared with three considered interconnections including Series-Parallel (SP), Bridge-Linked (BL), and Total-Cross-Tied (TCT). This, research work aims at computation and comparison of the performance of PV arrays though minimizing power losses, reducing multiple peaks in characteristic curve and improving the performance of power grid under different fault scenarios. Polycrystalline and CIGS PV technologies are considered for an in-depth analysis of the adopted methodology. The CIGS PV is a thin film material which is not widely used as compared to polycrystalline material. Therefore, it is worthwhile to consider the impact of faults with the adopted procedure on CIGS PV technology. It is found that the reconfigured PV array with CIGS materials is helpful in increasing the peak power.

Following are key contributions of this research paper:

(1). Minimization in power losses of PV array is achieved by adoption of reconfiguration method under various

fault scenarios. It should be noted that in the literature, the impact of different faults on reconfigured PV array with altering placement methods is not studied meticulously. Only the impact of shading is studied in the literature. The performance of the adopted reconfiguration method under short circuit faults is also investigated in this paper, which is not reported in the literature [20]–[32].

(2). Day-to-night transition fault is considered as a special case in which multiple faults are analyzed during the transition. The reconfiguration through suitable square matrix selection is not given due attention for analysis of multiple faults under shading conditions in the literature.

(3). Importantly, impact of all the studied faults on the power grid is well examined in this paper, which is not detailed in the previous works [20]–[32].

(4). The reconfiguration method is analyzed with CIGS thin film technology under various fault scenarios, which is not available in the literature.

(5). Different reconfiguration techniques like sudoku, optimal TCT, optimal sudoku, SD-PAR etc. [20]–[32] have only analyzed partial shading patterns in a PV array but this algorithm has not only been implemented under multiple faults scenario but also considered different PV technologies with different configurations.

The paper is organized as follows: System modeling of PV array under different faults and its grid connection is given in Section II. Current estimation and reconfiguration algorithm for considered PV array is deatiled in Section III. Simulations of the developed PV model with detailed discussion and anaylysis are given in Section IV. The paper is concluded in Section V.

II. SYSTEM MODELING

In this section, mathematical modeling of the studied PV array is presented for analysis of non-linear behavior of PV system during different fault scenarios. This section also explains different topologies of PV modules, and brief description of the investigated PV faults and the grid-connected PV system.

Different types of PV cell modeling techniques including five parameter model for single diode and seven parameters for double diode model are widely used in the literature. Five parameter model is chosen for this study in which a single solar PV cell is connected as a current source in parallel to the diode as shown in Figure 1, [35]. Where, shunt resistance is denoted by R_{sh}, and R_s shows series resistance. The value of n is taken close to 1 as an ideality factor. Referring to Eq. (1) and Eq. (2), I_{sc} represents short circuit current and T denotes operating temperature. STC stands for Standard Testing Condition. The value of Tr represents reference temperature, which is 25°C. The coefficient of I_{sc} is expressed as k_i 1000W/m^2. N_{sr} *and* N_{pa} represent number of interconnected series and parallel cells respectively. Energy band gap

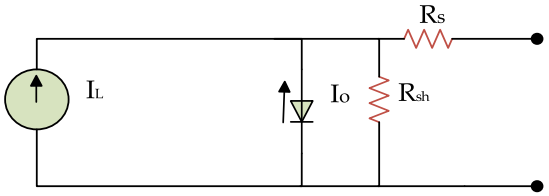

FIGURE 1. Equivalent cell modeling of a single PV cell.

of a semiconductor is represented by E_{go}. The output current of the PV module is represented by I_{pvm} as given in Eq. (1) which is light generated current of crystalline module. V_{oc} and I_{sc} are represent open-circuit voltage and short-circuit current respectively as given in Eq. (2) and Eq. (3), [35].

$$I_{pvm} = N_{pa} \times ([I_{sc} + k_i(T - T_r)]G_{STC}) - N_{pa} \times I_o \times \left[\exp\left(\frac{\frac{V}{N_{sr}} + \frac{I_{pvm} \times R_s}{N_{pa}}}{n \times V_t}\right) - 1\right] - \frac{V \times \frac{N_{pa}}{N_{sr}} + I_{pvm} \times R_s}{R_{sh}} \quad (1)$$

$$I_{sc} = N_{pa}\left(\frac{I_{STC}}{G_{STC}} \times G_R + k_i(T - T_{STC})\right) \quad (2)$$

$$V_{oc} = N_{sr}(V_{STC} + k_v(T - T_{STC}) + V_t \times \ln\left(\frac{I_{sc}/N_{pa}}{I_{STC}}\right) \quad (3)$$

where, I_{STC} and V_{STC} represent current and voltage at STC, resepctively. G_R is the received irradiance in W/m^2. k_V is the coefficient of open circuit voltage. The thermal voltage is characterized as V_t.

Solar arrays can be made up of PV cells with p-n homojunction (crystalline silicon) and p-n hetero-junction (CIGS). The homojunction solar cells like monocrystalline and polycrystalline PV cells follow the principle of superposition as light current can be expressed as uncorrelated sum of its diode current and constant photocurrent. On the other hand, hetero junction cells do not comply with superposition principle and may not be accurately described from the five parameter model. Authors in [39], [40] used a physics based model for heterojunction solar arrays for CIGS PV technology which computes irradiance and temperature dependent current-voltage parameters of PV array. J_{ph} or $I_{ph(CIGS)}$ represent the photocurrent due to photogenerated carriers of CIGS as given by Eq. (4). This current component depends upon irradiance and the applied voltage.

A CIGS cell consists of a zinc oxide (ZnO) window layer with wide band gap cadmium sulphide (CdS) buffer layer, stacked on top of CIGS absorber layer. The light generated current by CIGS is denoted by J_L or $I_{pv(CIGS)}$ as given in Eq. (5) [39], [40]. V_{oc} represent open circuit voltage

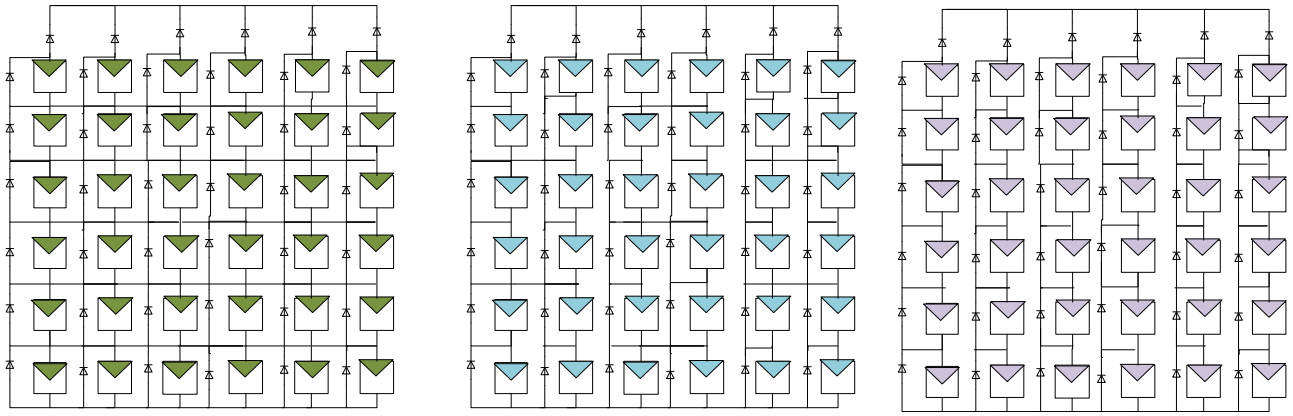

FIGURE 2. (a) TCT topology, (b) BL topology, (c) SP topology.

and Q is ideality factor of CIGS as presented in Eq. (6).

$$J_{ph} = J_{sc}\frac{1}{1+\alpha_c e^{\frac{q\beta(V-V_{bi})}{kT}}} \tag{4}$$

$$J_L = J_{ph} + J_0(e^{\frac{qV}{NkT}} - 1) + \left(G_{shunt} \times V + I_{Oshunt} \times V^{\gamma}\right) \tag{5}$$

$$V_{oc} = Q.\frac{kT}{q}.\ln\left(\frac{J_{ph}}{J_o}\right) \tag{6}$$

where, 'α_c' is the ratio between diffusion velocity and thermionic emission velocity. Voltage partition factor is denoted by 'β' which is assumed to be temperature independent [39]. G_{Shunt} and I_{OShunt} are the prefactors of linear and nonlinear shunt current, respectively, and γ is the power index of log shunt current. Value of V^{γ} denotes voltage with consideration of power index of log shunt current. J_o depends weakly on temperature and illumination which is diode saturation current for CIGS. Totally built in voltage of p-n junction V_{bi} is 0.6 V - 0.8 V. This physics based analytical model of CIGS solar array can help in development of basic understanding about the reliance of non-linear parameters of solar array on irradiance and temperature.

A. PV FAULTS SENARIOS

The studied faults include partial shading fault, bypass diode failure under shading, bridge fault under shading condition, bridge fault, and combined impact of short circuit, open circuit, bypass diodes defects and module mismatch faults. All the considered faults are thoroughly analyzed on polycrystalline and thin-film CIGS PV technology with three different interconnection topologies including Series-Parallel (SP), Bridge Linked (BL) and Total Cross Tied (TCT) as shown in Figure 2. SP is a commonly used topology in which PV modules are connected in series and parallel form while BL is a form of SP connection with more internal connections than that of SP, and in TCT toloplogy all the modules are closely tied together with more interconnections than SP and HC interconnections. The considered fault scenarios are shown in Figure 3.

Different types of the studied faults are as follows:

1) Partial shading fault (F1): It is a module mismatch fault which is analyzed under non-uniform shading pattern as shown in Figure 3.

2) Bypass diode failure under shading (F2): Defects of bypass diodes including reversal of connection and short circuit of bypass diode is analyzed under non-uniform shading in this fault scenario.

3) Bridge fault under shading condition (F3): Short circuit among different PV strings develop bridge fault. It is analyzed under non-uniform shading.

4) Bridge fault (F4): In this fault scenario, individual bridge fault is analyzed. Impact of bridge fault on a PV array without partial shading is analyzed in this fault scenario.

5) Combined impact of faults (F5): In this scenario, combined impact of all the faults including short circuit, open circuit, bypass diodes defects and module mismatch due to shading is analyzed. Combined impact of faults also includes a special case of day to night transition fault in which multiple faults are considered under partial shading condition.

The impact of all considered cases of faults are also analyzed on power grid. Block diagram of grid connected PV array is shown in Figure 4, in which considered PV array is connected to 25 kW grid model through inverter and dc-to-dc booster. The employed MPPT controller takes value of V_{pv} and I_{pv} from the PV panel to track peak power through adjustment of duty cycle by changing level of voltage V, [33], [34]. The level of voltage will change in the same direction as of the power increase. The dc-to-dc booster is integral for increasing the voltage after extracting D control pulses through MPPT [35].

III. ROW CURRENT ESTIMATION

Assessment of performance of the adopted interconnections and reconfiguration method (RM) is performed through computation of current equations. The equations for a row current at STC is represented with I_m as the module current. As we know that sudden decrease in current due to harsh environmental conditions can decrease output power

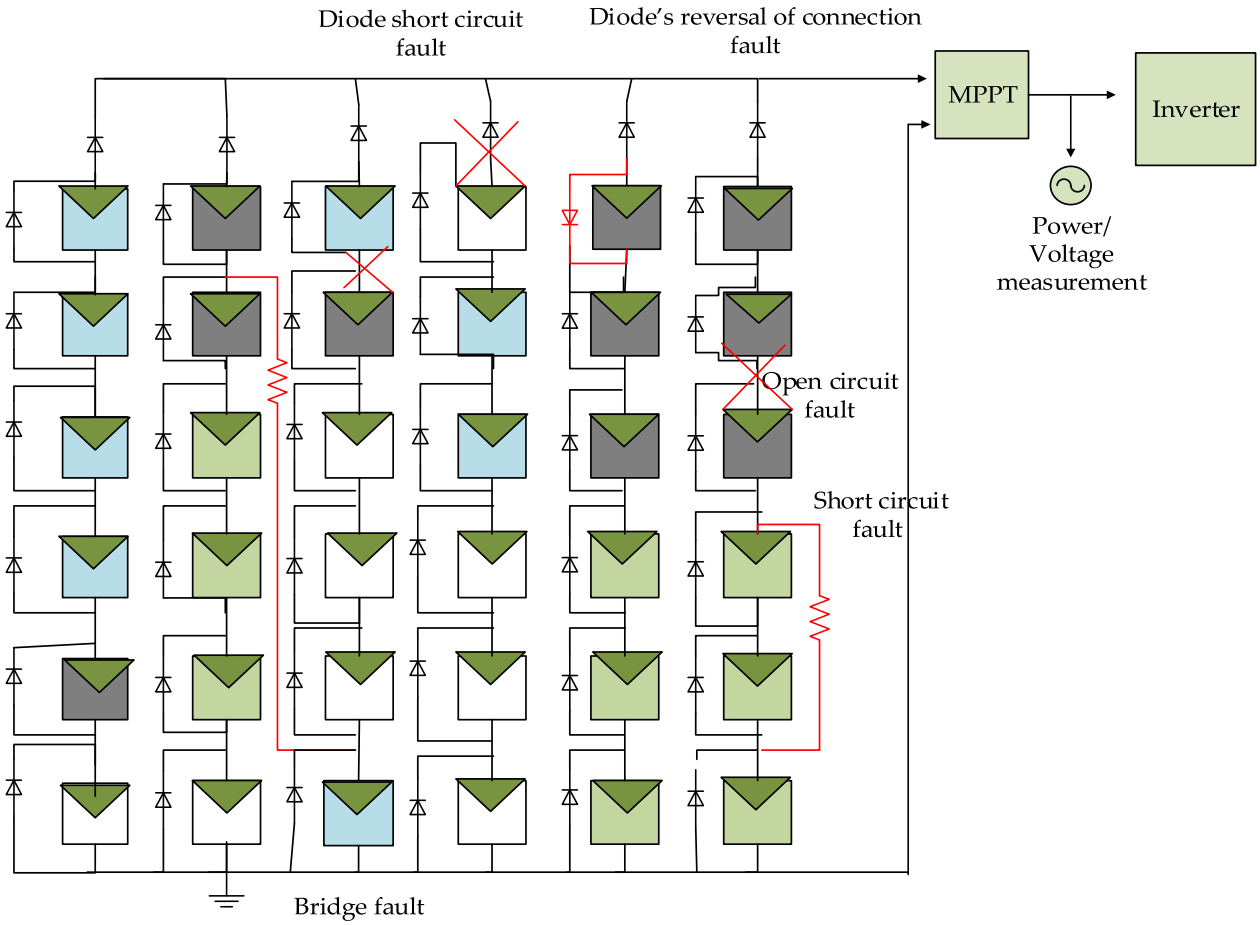

FIGURE 3. Considered faults in PV array.

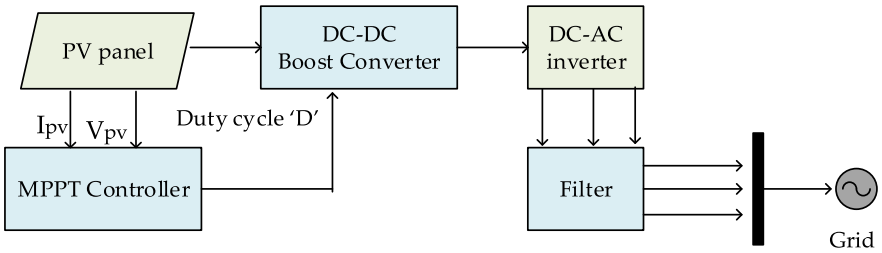

FIGURE 4. Block diagram of grid-connected PV system.

significantly. The adopted reconfiguration method through physical relocation of PV modules does not only compensate the sudden decrease of current due to fault occurrence but also optimize the power peak with minimization of multiple peaks in the curve. Algorithm of the developed scheme is shown in Figure 5.

$$\mathrm{I} = \left(\frac{\mathrm{G_R}}{\mathrm{G_{STC}}}\right) \times I_{\mathrm{m}} \tag{7}$$

$$I_{R1} = \left(\left(4 \times \frac{500}{1000} \times I_{1n}\right)\left(1 \times \frac{700}{1000} \times I_{1n}\right) \times \left(1 \times \frac{1000}{1000} \times I_{1n}\right)\right) = 3.7I_{1n} \tag{8}$$

$$I_{R2} = \left(\left(3 \times \frac{400}{1000} \times I_{1n}\right)\left(2 \times \frac{700}{1000} \times I_{1n}\right) \times \left(1 \times \frac{1000}{1000} \times I_{1n}\right)\right) = 3.6I_{1n} \tag{9}$$

$$I_{R3} = \left(\left(2 \times \frac{500}{1000} \times I_{1n}\right)\left(1 \times \frac{700}{1000} \times I_{1n}\right) \times \left(3 \times \frac{1000}{1000} \times I_{1n}\right)\right) = 4.7I_{1n} \tag{10}$$

$$I_{R4} = \left(\left(2 \times \frac{500}{1000} \times I_{1n}\right)\left(4 \times \frac{1000}{1000} \times I_{1n}\right)\right) = 5I_{1n} \tag{11}$$

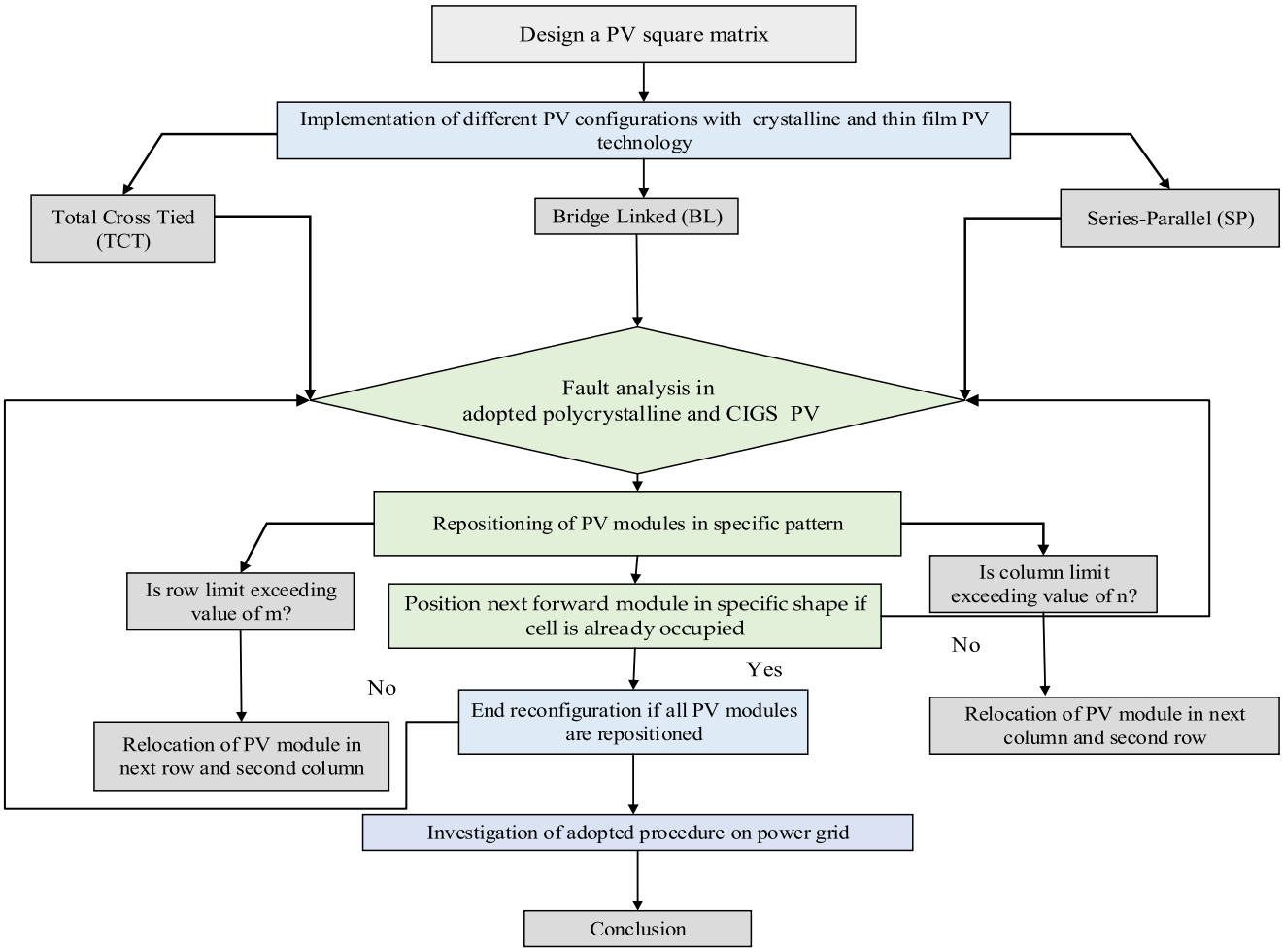

FIGURE 5. Algorithm of the developed scheme.

The estimated current for row 5 'I_{R5}'and row 6 'I_{R6}' is computed in Eq. (12) and Eq. (13) as follows:

$$I_{R5} = \left(\left(3 \times \frac{400}{1000} \times I_{1n}\right)\left(3 \times \frac{700}{1000} \times I_{1n}\right)\right) = 3.3I_{1n} \tag{12}$$

$$I_{R6} = \left(\left(3 \times \frac{400}{1000} \times I_{1n}\right)\left(3 \times \frac{700}{1000} \times I_{1n}\right)\right) = 3.3I_{1n} \tag{13}$$

The estimation of row current is considered important for PV module mismatch fault. Row current estimation helps to evaluate difference between each row current. The difference between estimated values of row current shows the amount of shade dispersion. It is know that sudden decrease in current occurs due various faults under partial shading conditoins leading to significant power losses. The row current for 6×6 PV array without reconfiguration is caluculated using Eq. (7), [22]. The estimated value of current of all rows before reconfiguration is computed using Eq. (8) to Eq. (13).

A reconfiguration method (RM) of number placement is adopted to optimize the PV performance under different fault scenarios as shown in Figure 6.

The PV modules are optimally placed through this number placement method. Irradiance is uniformly poised by adoption of this method and the impact of faults is significantly reduced. The estimation of row current is performed for adopted procedure in next section to assess the performance of the adopted interconnections and the reconfiguration method. The reconfiguration technique prevents the sudden difference and decrease in current through physical relocation of PV modules and helps to achieve global maxima and optimize the overall performance of PV system. Sudden difference in row currents due to change in irradiance is evident from all the presented values.

A. RECONFIGURATION OF PV ARRAY

Number placement of a square matrix is performed in this study. A puzzle square pattern is followed which uses a number placement [22] that positions the modules in a specific pattern. Positioning refers to arrangement of PV modules in

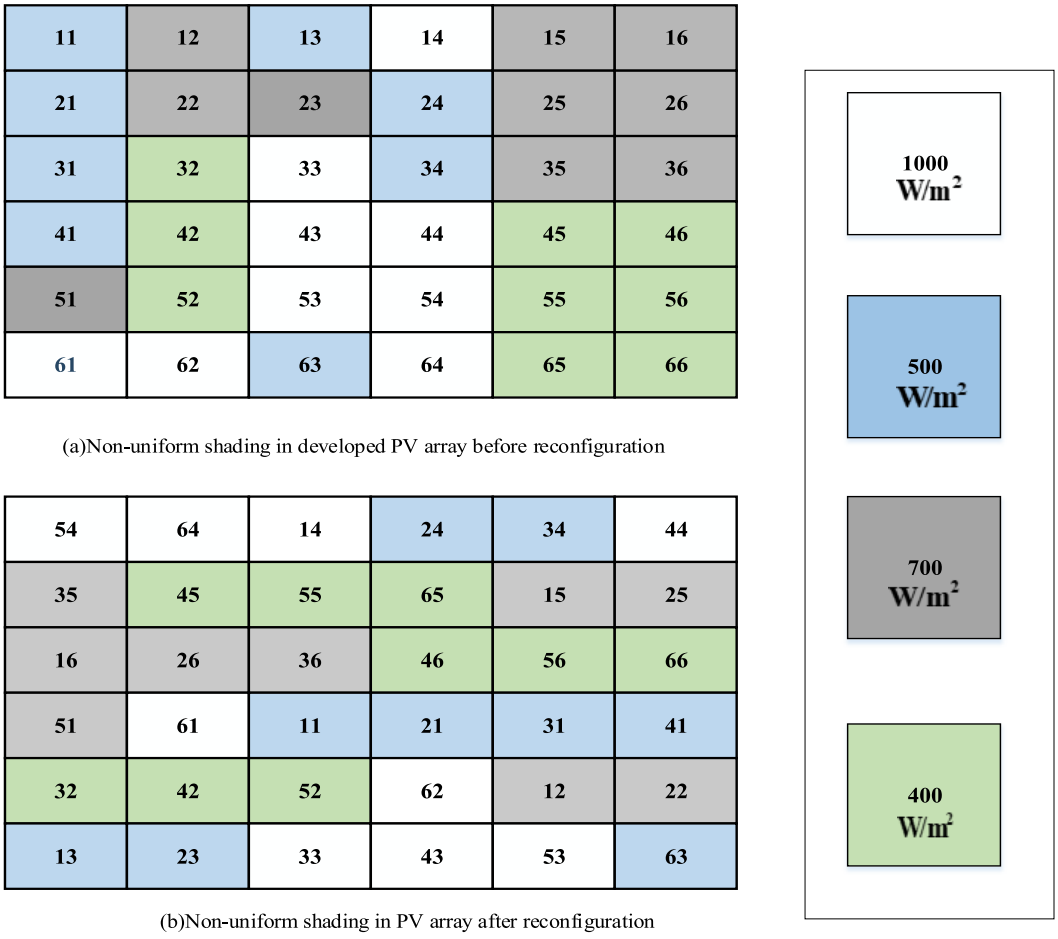

FIGURE 6. Array arrangement before and after reconfiguration of PV array.

series parallel connection. Important considerations to reconfigure the PV array are as follows:

11 refers to position of PV module at first row and first column and is continued so. The first repositioning of modules is a random optimal choice and any position can be allotted to the first module over entire array dependending upon the fault condition. The subsequent number i.e. 12 will follow the structure of **L** shape and its updated position will be 55 as indicated in Figure 6. The detailed steps of reconfiguration are also elaborated in layout of developed scheme. If any number encounters oversteps i.e. m > 6 then resume the series from the next row an second column. If any column limit i.e. $n > 6$ is exceeded then resume the series from the second column with the next row position. Each module is shuffled with this method. The estimated current for row 1&2 i.e. I_{R1} and I_{R2} after applying reconfiguration method (RM) to minimize the difference between currents are computed using Eq. (14) and Eq. (15) respectively.

$$I_{R1} = \left(\left(1 \times \frac{500}{1000}\right)\left(3 \times \frac{700}{1000}\right)\left(1 \times \frac{1000}{1000}\right) \times \left(1 \times \frac{400}{1000}\right) \times I_{1n}\right) = 4I_{1n} \quad (14)$$

$$I_{R2} = \left(\left(1 \times \frac{500}{1000} \times I_{1n}\right)\left(1 \times \frac{700}{1000} \times I_{1n}\right) \times \left(2 \times \frac{1000}{1000} \times I_{1n}\right)\left(2 \times \frac{400}{1000}\right)\right) = 4I_{1n} \quad (15)$$

The current value for row 3, i.e. I_{R3} and row 4, i.e. I_{R4} is computed in Eq. (16) and Eq. (17) as follows:

$$I_{R3} = \left(\left(1 \times \frac{500}{1000} \times I_{1n}\right)\left(1 \times \frac{700}{1000} \times I_{1n}\right) \times \left(2 \times \frac{1000}{1000} \times I_{1n}\right)\left(2 \times \frac{400}{1000}\right)\right) = 4I_{1n} \quad (16)$$

$$I_{R4} = \left(\left(2 \times \frac{500}{1000} \times I_{1n}\right)\left(2 \times \frac{400}{1000} \times I_{1n}\right) \times \left(2 \times \frac{1000}{1000} \times I_{1n}\right)\right) = 3.8I_{1n} \quad (17)$$

The computed current for row 5 'I_{R5}'and row 6 'I_{R6}' is estimated in Eq. (18) and Eq. (19) as follows:

$$I_{R5} = \left(\left(2 \times \frac{500}{1000}\right)\left(2 \times \frac{700}{1000}\right)\left(1 \times \frac{1000}{1000}\right) \times \left(1 \times \frac{400}{1000}\right)\right) \times I_{1n} = 3.8I_{1n} \quad (18)$$

TABLE 2. Parameters of the studied PV modules.

Sr. No.	Parameter	Polycrystalline PV module	CIGS PV module
1	Open-circuit voltage V_{oc} (V)	36.5	63.2
2	Short-circuit current I_{sc} (A)	8.26	6.1
3	Max. peak power $P_{\max}$ (W)	225	225
4	Max. peak voltage V_{mp} (V)	29.2	45
5	Max. peak current I_{mp} (A)	7.7	5
6	photocurrent I_L (A)	8.26	6.33
7	Diode saturation current I_o (A)	1.39×10^{-10}	2.17×10^{-10}
8	Diode ideality factor n	0.95	0.95
9	Shunt resistance R_{sh} (Ω)	476.1	56.1
10	Series Resistance R_s (Ω)	0.41	2.1

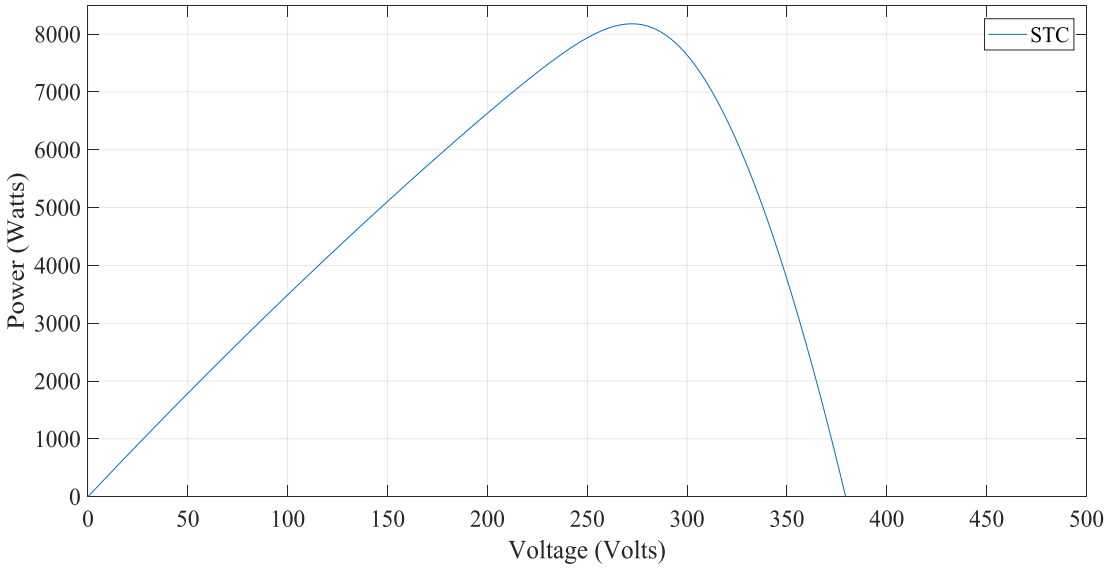

FIGURE 7. P-V curve under fault free operation.

$$I_{R6} = \left(\left(2 \times \frac{500}{1000}\right)\left(2 \times \frac{700}{1000}\right)\left(1 \times \frac{1000}{1000}\right) \times \left(1 \times \frac{400}{1000}\right) I_{1n}\right) = 3.8 I_{1n} \quad (19)$$

The RM procedure decreases the sudden difference between current values as shown from the above equations. The row currents computed after reconfiguration show small and negligible changes in the current values under module mismatch faults which will help minimizing the impact of faults. This evaluation will be further validated by simulation results. The obtained results are analyzed and discussed in next section.

IV. SIMULATIONS

A Simulink model of a 6 × 6 PV array under various faults is developed to study the performance of PV array under considered fault scenarios. This 6 × 6 PV array is modeled in MATLAB with a single PV module of 225 Watts. The specifications of the considered PV module are given in Table 2. A fault free operation of 6 × 6 PV array at STC is considered for finding the maximum power peak. Total peak power generated in fault free operation is 8.1 kW as shown in Figure 7.

A. PARTIAL SHADING FAULT (F1)

Non-uniform shading pattern is analyzed with the three different interconnections during this fault as shown in Figure 8. The computed parameters of PV model under 'F1' secanio is given in Table 3. Sudden multiple power peaks appeared in the curve due to sudden decrease in current. The peak power reduced from 8.1 kW to 4.6 kW in TCT, 4 kW in

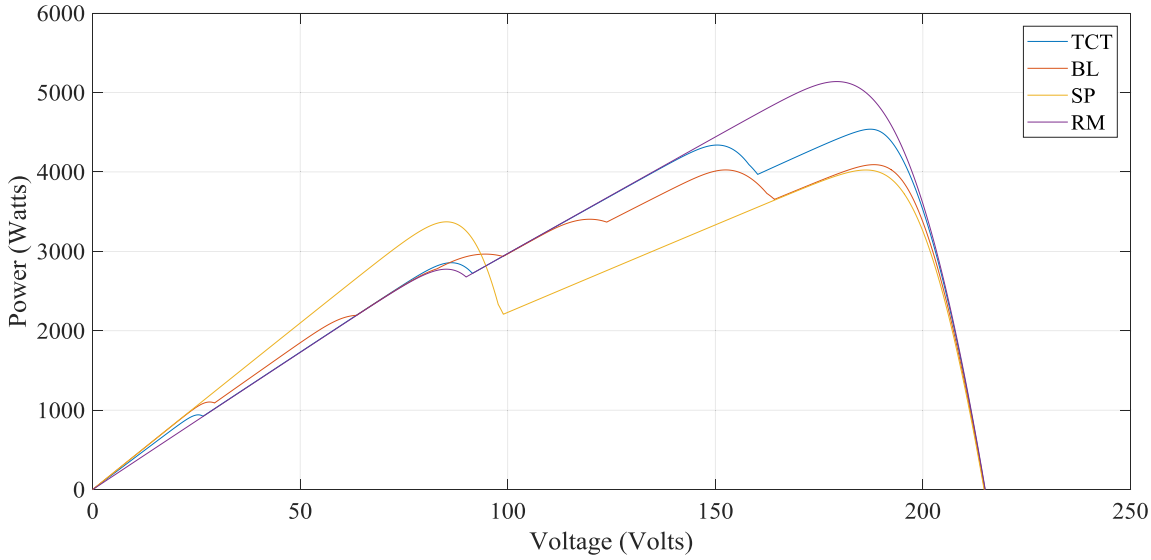

FIGURE 8. P-V curve under partial shading fault 'F1' (polycrystalline).

TABLE 3. Computations of PV model under partial shading fault (F1).

Topology	Maximum peak Power (kW)	Maximum peak voltage (V)	Maximum peak current (A)
		Polycrystalline PV	
TCT	4.6	180	25.5
BL	4.01	185	21.2
SP	3.99	186	21.4
RM	5.04	172	29.3
		CIGS PV	
TCT	4.94	300	16.4
BL	4.72	300	15.7
SP	4.68	300	15.6
RM	5.21	289	18

BL and 3.98 kW in SP with multiple peaks in the curve. After applying RM, the peak power increases to 5.01 kW in polycrystalline PV module. The results further improved for the CIGS thin film material as shown in Figure 9.

It is evident that CIGS performs better than polycrystalline and improves power peak with 4.9 kW in TCT, 4.25 kW in BL and 4.2 kW in SP interconnection. The adopted RM procedure improves the performance with increase in power peak to 5.2 kW. It can also be observed that TCT performs better than that of BL and SP topologies. The power loss further minimized after suitable positioning of PV modules, and the multiple peaks are reduced with ceratin increase in the peak power.

B. BYPASS DIODE FAILURE UNDER SHADING (F2)

Defects of bypass diodes including reversal of connection and short circuit of bypass diode is analyzed under non-uniform shading as shown in Figure 10 and 11 which demonstarte that power is reduced to 3.6 kW in SP, 3.56 kW in HC and 3.64 kW in TCT interconnection. The computed values of PV model under 'F2' case is given in Table 4.

It is seen that more peak power is achieved in BL interconnection than SP and TCT interconnection through adoption of CIGS PV technology but multiple peaks appear in both SP and BL interconnections which is not desirable. TCT interconnection reduces the number of peaks but decreases the power output. The adoption of RM not only increases the peak power but also reduces number of peaks in both polycrystalline and CIGS material.

C. BRIDGE FAULT UNDER SHADING CONDITION (F3)

Impact of bridge fault under non-uniform shading is analyzed in this fault scenario. TCT interconnection performs better than other interconnections in terms of minimization of power losses. Figure 12 and Figure 13 show that the maximum peak power (MPP) increases from 3.1 kW in SP, 3.4 kW in TCT

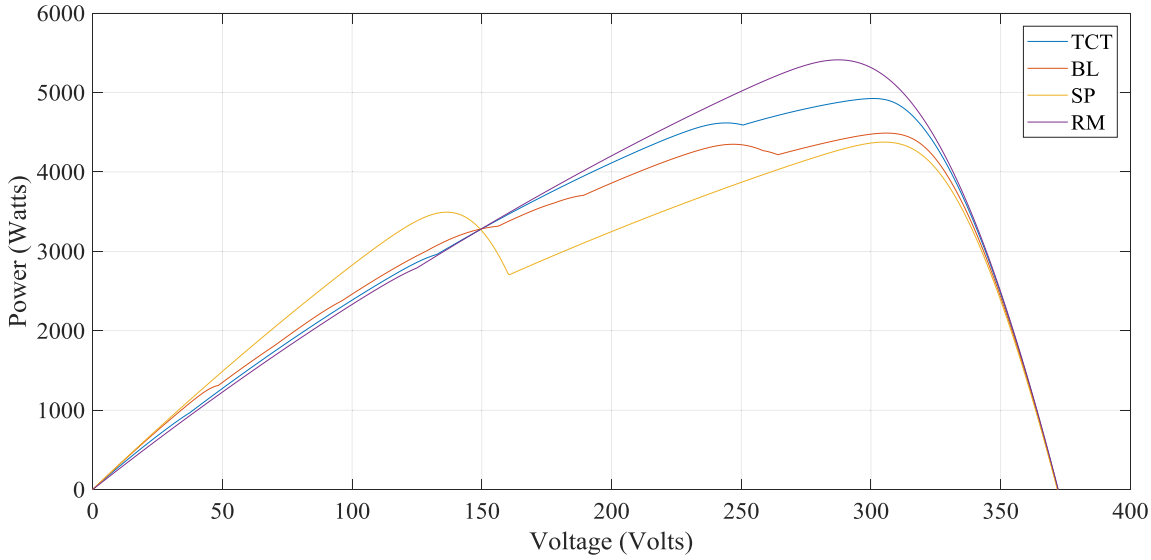

FIGURE 9. P-V curve under partial shading fault 'F1' (CIGS).

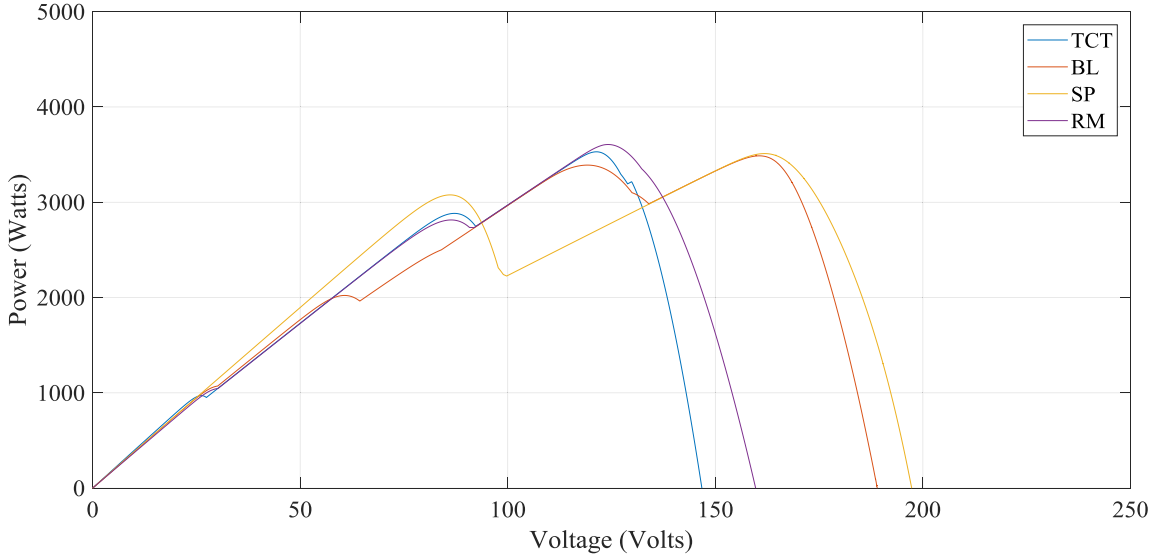

FIGURE 10. P-V curve for bypass diode faults under partial shading 'F2' (Polycrystalline).

and 3.39 kW in BL with polycrystalline PV. The multiple peaks disappeared after applying RM with increase in power to 4.05 kW. The computed values of PV model under 'F3' is given in Table 5.

D. BRIDGE FAULT (F4)

The results of bridge fault 'F4' are shown in Figure 14 and Figure 15. It becomes evident that SP interconnection outperforms the other interconnections with minimization of power losses. The maximum peak power (MPP) decreases from 5.75 kW in SP, 5.4 kW in TCT, and 5.7 kW in BL with polycrystalline PV. The CIGS PV produces 5.8 kW in TCT, 6.15 kW in BL and 6.3 kW in SP, whereas RM produces approximately the same power peak as SP interconnection i.e. 3.6 kW. It is found that the RM procedure cannot minimize power losses of PV array during bridge fault as there are no multiple peaks in its power-voltage curve. However, application of RM algorithm certainly optimizes the performance of PV arrays by minimizing sudden decrease in the current which may not be achieved in F4 as the bridge fault (F4) does not produce multiple peaks in its characteristic curve. Thus, the proposed algorithm has the ability to effectively minimize the impact of multiple faults and shading conditions where sudden decrease in the current develops multiple peaks in the characteristic curve. The computed values of PV model under 'F4' is given in Table 6.

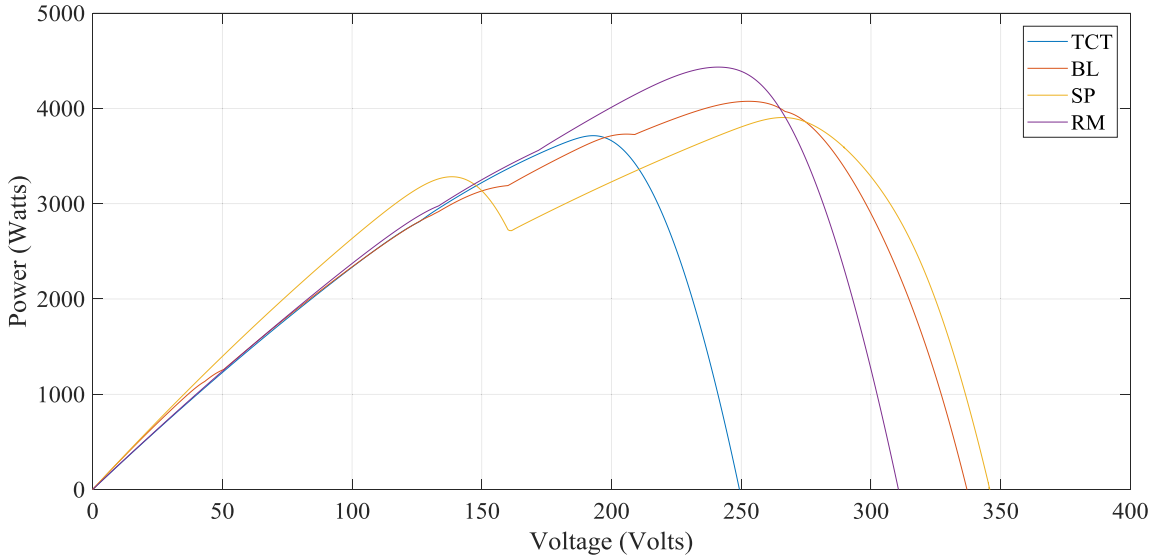

FIGURE 11. P-V curve for bypass diode faults under partial shading 'F2' (CIGS (TF)).

TABLE 4. Computation of PV model for bypass diode failure under shading (F2).

Topology	Maximum peak power (kW)	Maximum peak voltage (V)	Maximum peak current (A)
		Polycrystalline PV	
TCT	3.6	125	28.8
BL	3.42	160	21.37
SP	3.6	160	22.5
RM	3.71	125	29.6
		CIGS PV	
TCT	3.70	200	18.7
BL	3.94	250	15.76
SP	3.87	254	15.2
RM	4.23	240	17.8

TABLE 5. Computation of PV model for bridge fault under shading (F3).

Topology	Maximum peak power (kW)	Maximum peak voltage (V)	Maximum peak current (A)
		Polycrystalline PV	
TCT	3.44	140	24.57
HC	3.3	140	23.5
SP	3.21	140	22.9
RM	4.1	150	27.3
		CIGS PV	
TCT	4.02	250	16.08
HC	4.1	245	16.4
SP	4.0	298	14
RM	4.35	248	17.54

E. COMBINED IMPACT OF FAULT (F5)

Impact of all the faults is analyzed in this case for performance evaluation of the applied algorithm under the stidied faults scenarios. It is found that the power reduced from 8 kW to 3.1 kW in SP, 3.23 kW in HC and 3.33 kW in TCT as shown in Figure 16 and Figure 17. The power is optimized

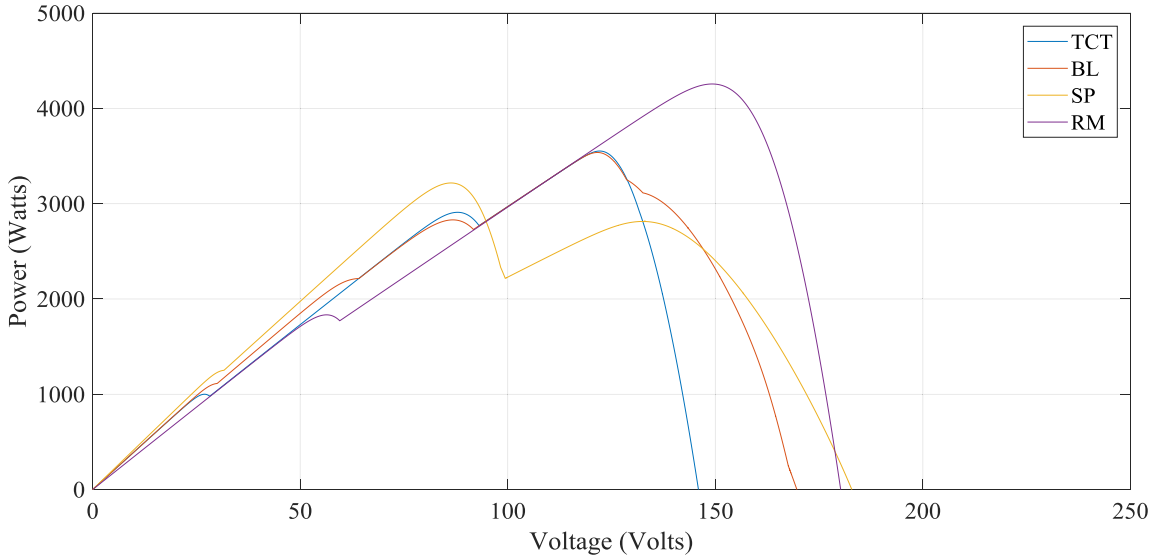

FIGURE 12. P-V curve for bridge fault under shading 'F3' (polycrystalline).

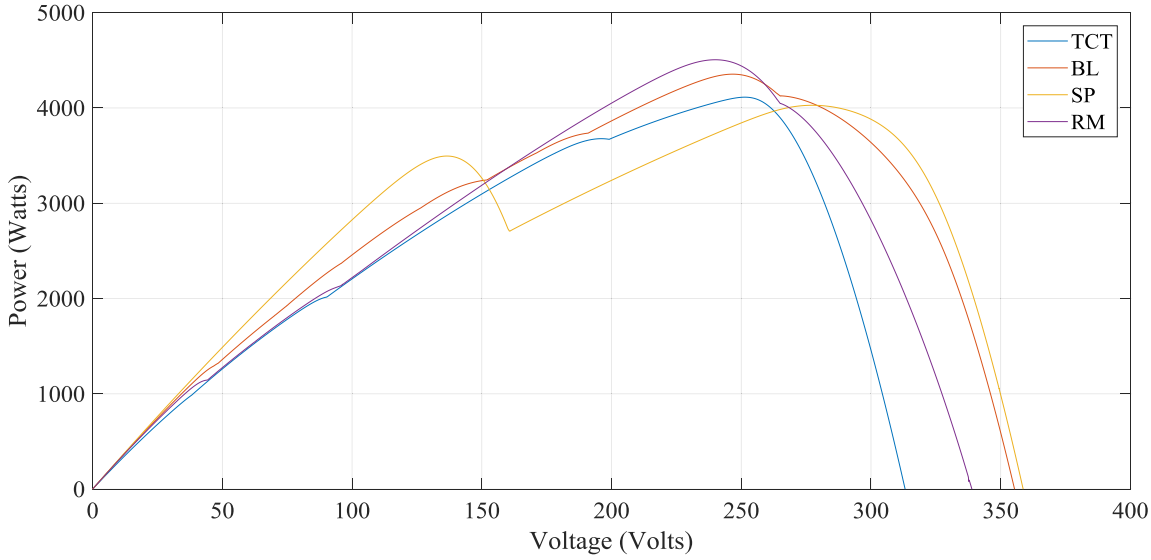

FIGURE 13. P-V curve for bridge fault under shading 'F3' (CIGS(TF)).

after applying RM from 3.33 kW to 3.45 kW with multiple peak minimization. It becomes visible that thin film (CIGS) performs better than crystalline PV array in this scenario and generates single global peak in P-V curve. The computed values of PV model under 'F5' are given in Table 7.

It may be noted that CIGS PV accomplishes better under all fault scenarios than monocrystalline PV material according to P-V curve analysis in terms of maximum power generation. The impact of thin film and monocrystalline PV in adopted interconnections on the performance of the power grid is also analyzed to make the presented investigation more inclusive.

F. IMPACT OF PV FAULTS ON POWER GRID

In this sub-section, the impact of all considered faults on power grid is analyzed. The operation of the developed system is analyzed under STC for fault free operation as shown in Figure 18.

The MPP starts regulating through varying duty cycle after enabling MPPT at nearly 3100ms. Nearly 8kW MPP is tracked with a tracking time of approximately 3200 ms and continues to track MPP till the end under nominal condition i.e. 1000 W/m^2 and 25°C. This MPPT procedure improves peak power but it is not efficient enough to track global peak in a shifting environment. Installation of overcurrent protection devices (OCPD) in PV systems are helpful in clearing fault but multiple faults have small current losses under shading conditions which cannot be detected easily. The adopted methodology invloves reconfiguration method for SP, BL and TCT interconnections. It is seen that peak power gets reduced from 8 kW to 3.6 kW under non-uniform

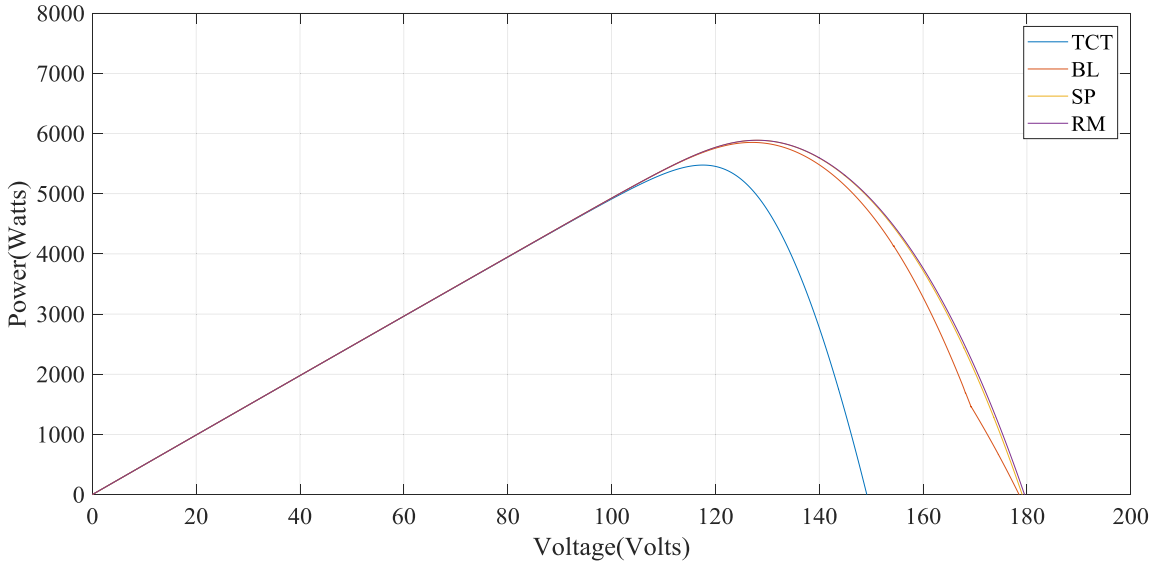

FIGURE 14. P-V curve for bridge fault 'F4' (polycrystalline).

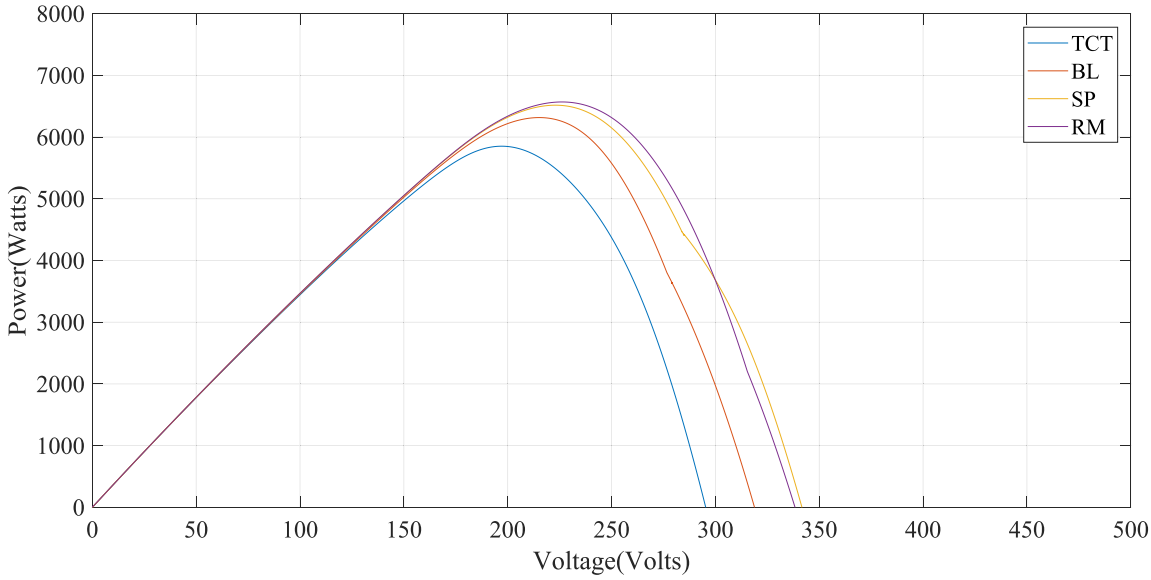

FIGURE 15. P-V curve for bridge fault 'F4' (CIGS).

shading 'F1' of polycrystalline PV array with SP interconnection. Power output increases from 3.6 kW to 3.8 kW on BL interconnection. The TCT arrangement optimizes the peak power to 4.0 kW and 4.5 kW after applying RM procedure with MPPT enabled at 3000 ms. The CIGS PV array performs better than polycrystalline and increases tracked MPP from 3.9 kW to 4.0 kW in BL interconnection. The peak power increases from 3.6 kW to 3.9 kW in SP interconnection. The TCT arrangement optimizes the peak power from 4.0 kW to 4.4 kW. Peak power of approximately 4.8 kW is achieved after applying RM procedure with enabled MPPT at 3000ms as shown in Figure 19 and Figure 20.

The bypass diode fault under shading 'F2' with polycrystalline PV array reduced tracked MPP from 8 kW to 3.4 kW, and 3.3 kW in SP and BL interconnections respectively. The TCT arrangement gives approximately same peak power as SP i.e. 3.4 kW. The peak power increased from 3.4 kW to 3.8 kW after applying RM procedure. The CIGS PV array performs better than polycrystalline and increases peak power from 3.4 kW to 3.7 kW in BL and 3.3 kW to 3.6 kW in SP interconnection respectively. Approximately 3.5 kW peak power is achieved under TCT arrangement. The peak power increased from 3.5 kW to 4.1 kW after applying RM as depicted in Figure 21 and Figure 22.

TABLE 6. Computations of PV model for bridge fault (F4).

Topology	Maximum peak power (kW)	Maximum peak voltage (V)	Maximum peak current (A)
		Polycrystalline PV	
TCT	5.4	119	45.3
BL	5.70	130	43.8
SP	5.75	130.09	44.3
RM	5.77	130.1	44.3
		CIGS PV	
TCT	5.8	200	29
BL	6.15	219	28.0
SP	6.3	223	28.2
RM	6.36	225	28.26

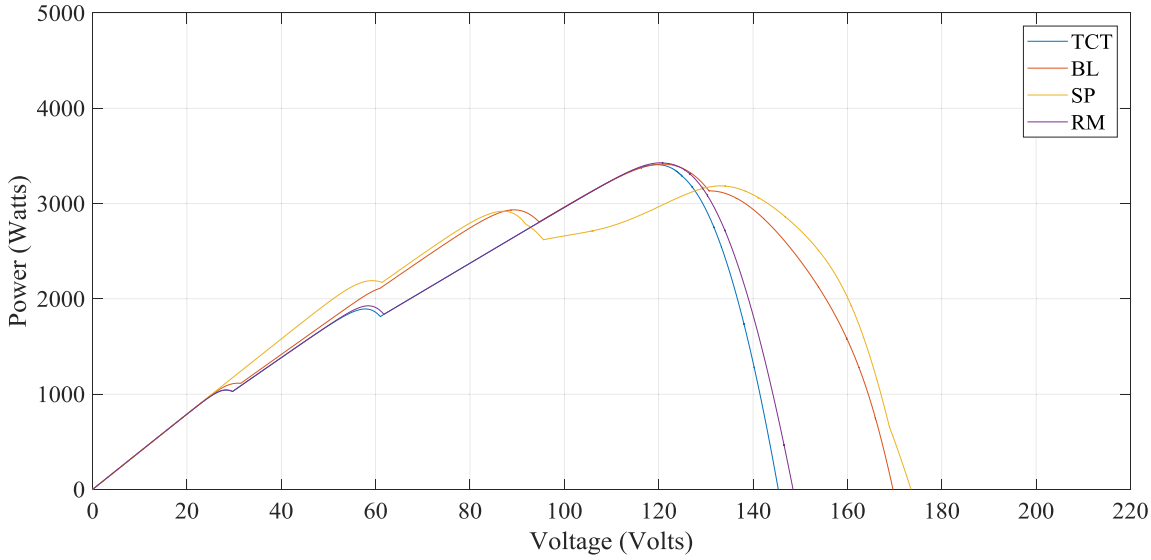

FIGURE 16. PV curve for combined impact of fault 'F5' (polycrystalline).

TABLE 7. Computations of PV model for combined impact of fault (F5).

Topology	Maximum peak power (kW)	Maximum peak voltage (V)	Maximum peak current (A)
		Polycrystalline PV	
TCT	3.33	125	26.4
BL	3.23	160	20.1
SP	3.1	160	19.37
RM	3.45	126	27.3
		CIGS PV	
TCT	3.6	200	18
BL	3.52	200	17.6
SP	3.44	204	16.86
RM	3.73	249	14.9

The bridge fault under shading 'F3' with polycrystalline PV array reduces MPP from 8 kW to 3.0 kW and 2.6 kW in BL and SP interconnections respectively. The TCT arrangement optimizes the peak power to 3.3 kW and 3.7 kW after applying RM procedure after enabling MPPT at 3100 ms and continues to tracked decreased power until end due to

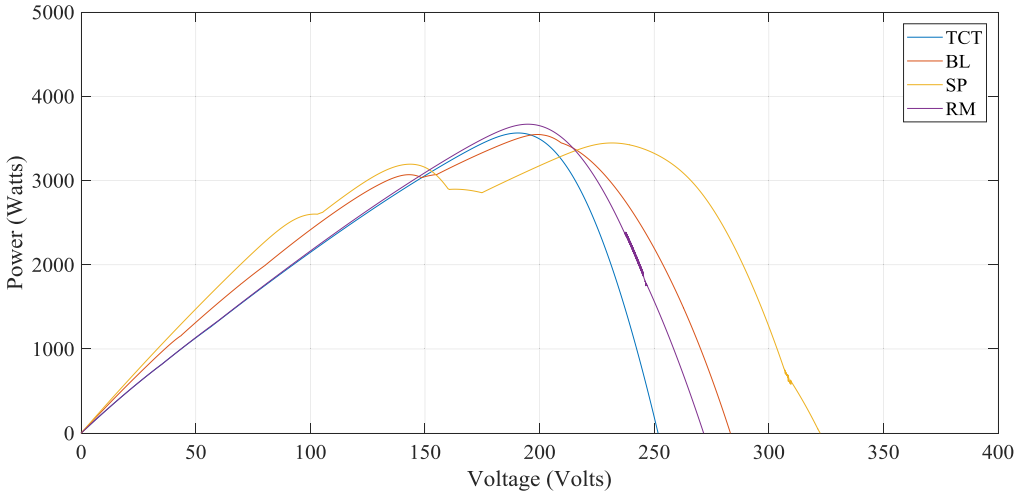

FIGURE 17. PV curve for Combined impact of faults 'F5' on CIGS (TF).

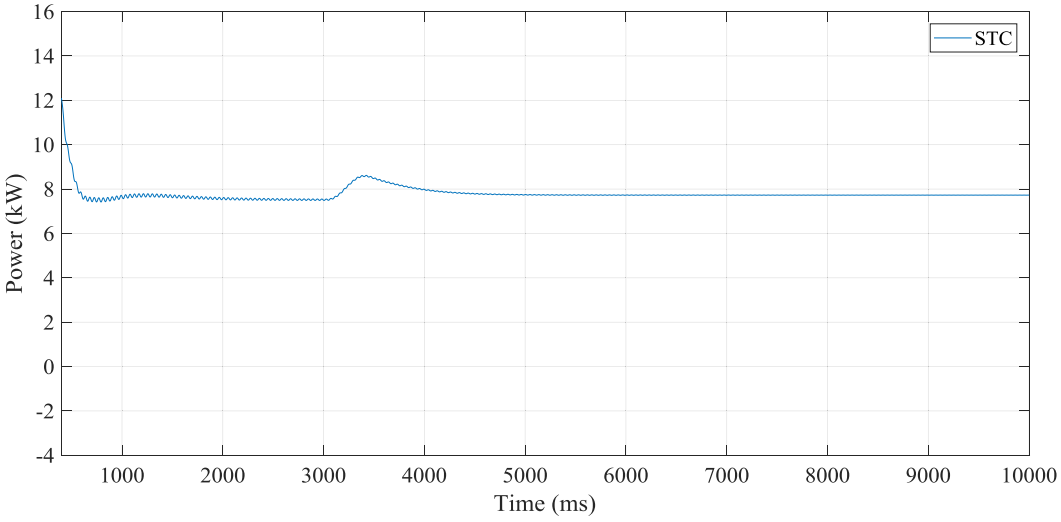

FIGURE 18. Power grid under STC (1000W/m^2 and *25°C*).

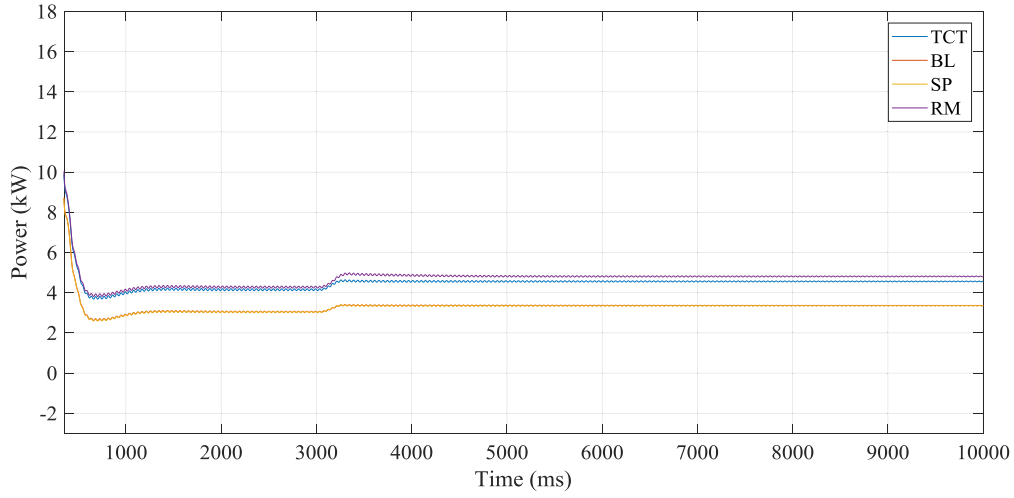

FIGURE 19. Impact of partial shading 'F1' on power grid (polycrystalline).

introduced fault. The CIGS PV array performs better than polycrystalline and increases peak power from 2.6 kW to 3.5 kW in SP interconnection. Peak power increases from 3.0 kW to 3.5 kW in BL interconnection. The TCT arrangement enhances the peak power to 3.84 kW and 3.9 kW after applying RM procedure as evident from Figure. 23 and Figure. 24.

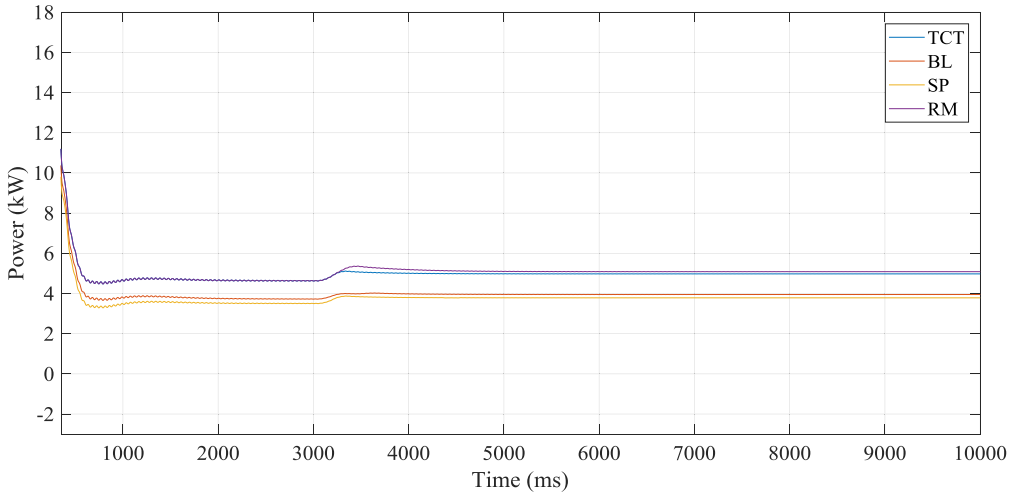

FIGURE 20. Impact of partial shading 'F1' on power grid (CIGS).

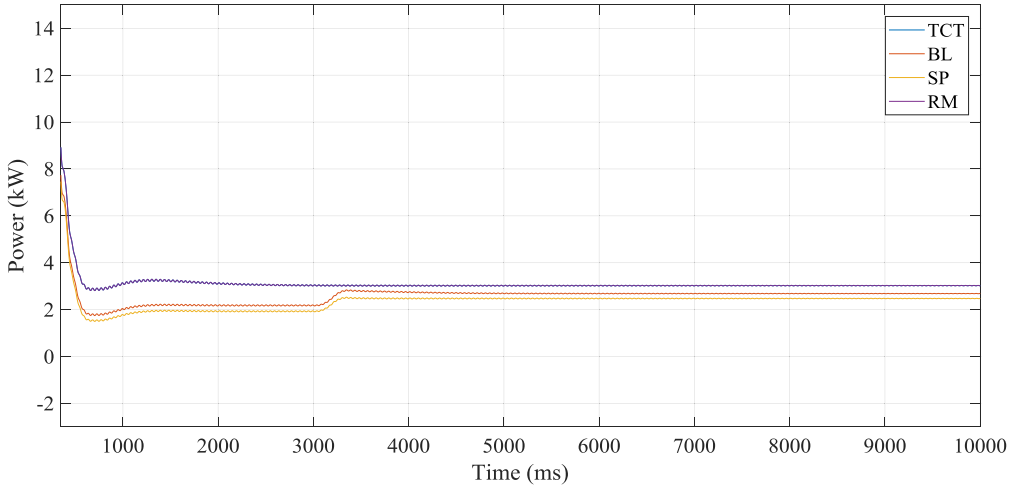

FIGURE 21. Impact of bypass diode failure under shading (F2) on power grid (polycrystalline).

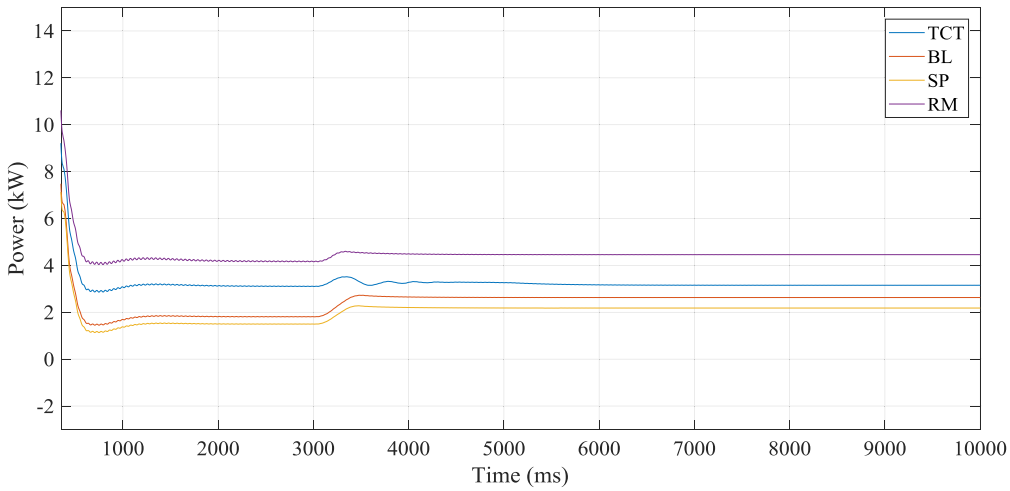

FIGURE 22. Impact of bypass diode failure under shading 'F2' on power grid (CIGS).

The bridge fault 'F4' in polycrystalline PV array decreases peak power from 8 kW to 4.7 kW and 4.5 kW in BL and TCT interconnections respectively. The SP arrangement gives the peak power up to 5.19 kW and remains unchanged after applying RM procedure. The CIGS PV array perform better than polycrystalline and increases tracked MPP

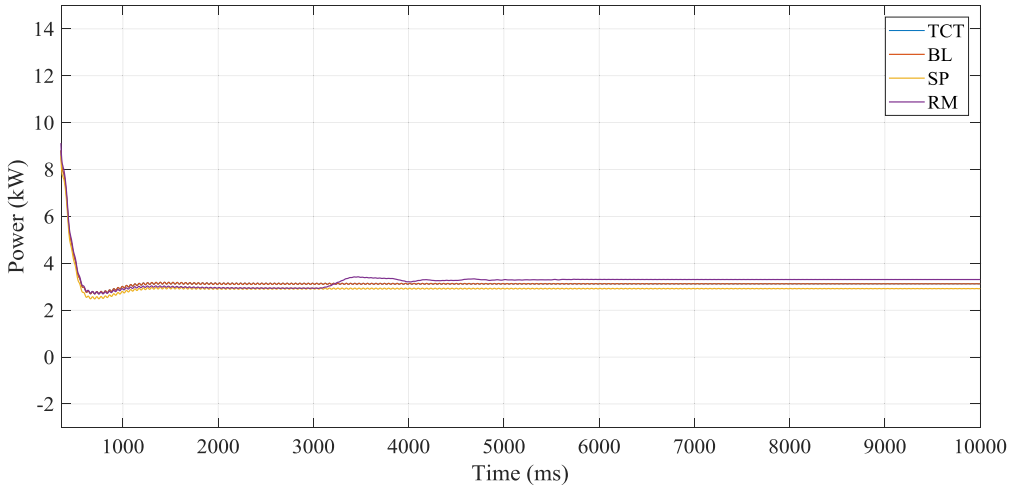

FIGURE 23. Impact of bridge fault under shading 'F3' on power grid (polycrystalline).

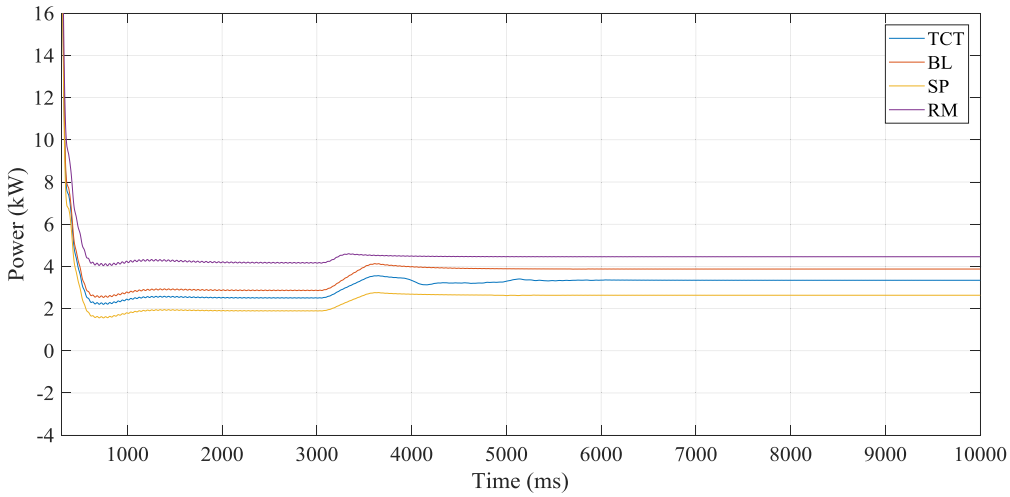

FIGURE 24. Impact of bridge fault under shading 'F3' on power grid (CIGS).

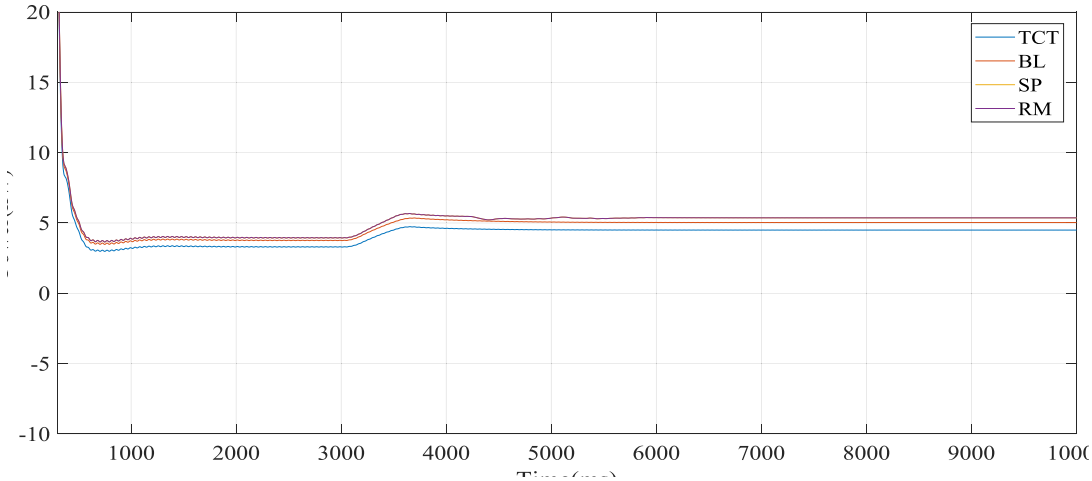

FIGURE 25. Impact of bridge fault 'F4' on power grid (polycrystalline).

from 4.5 kW to 5.23 kW, and 4.85 kW in BL and TCT interconnection respectively. The SP arrangement optimizes the peak power to 5.3 kW and 5.37 kW after applying RM procedure as depicted in Figure 25 and Figure 26.

The combined fault 'F5' with polycrystalline PV array reduces MPP from 8 kW to 3.2 kW and 3.0 kW in BL and SP interconnections respectively. The TCT arrangement optimizes the peak power to 3.3 kW and 3.6 kW after applying RM procedure.

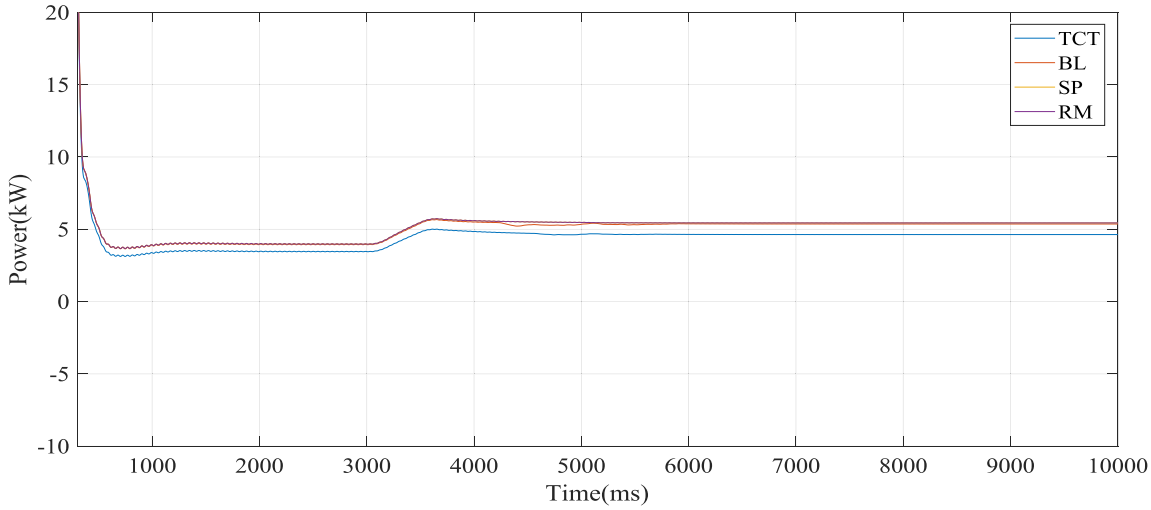

FIGURE 26. Impact of bridge fault 'F4' on power grid (CIGS (TF)).

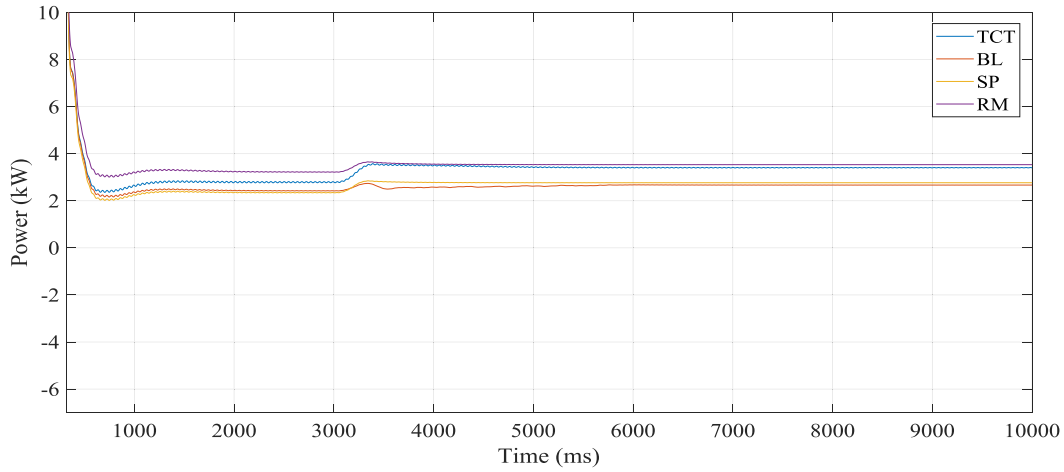

FIGURE 27. Combined impact of fault 'F5' on power grid (polycrystalline).

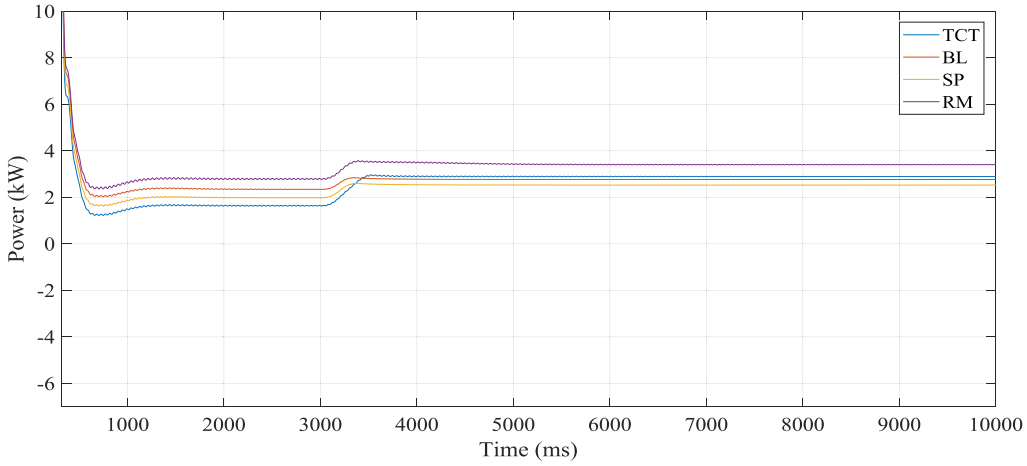

FIGURE 28. Combined impact of fault 'F5' on power grid (CIGS).

The CIGS PV array performs better than polycrystalline and increases tracked peak power from 3.2 kW to 3.4 kW and 3.56 kW in BL and SP interconnections respectively. The TCT arrangement enhances the peak power to 3.7 kW and 3.8 kW after applying RM procedure as revealed in Figure. 27 and Figure. 28.

TABLE 8. Comparison of the studied interconnections in PV array.

Studied Faults (F)	P_{max} in fault scenarios (kW)							
	Polycrystalline PV				CIGS PV			
	SP	BL	TCT	RM	SP	BL	TCT	RM
F1	3.99	4	4.6	5.02	4.2	4.3	4.9	5.12
F2	3.55	3.45	3.5	4.1	4	3.9	3.85	4.5
F3	2.9	3.32	3.65	4	3.7	3.82	4.05	4.15
F4	5.75	5.7	5.4	5.77	6.3	6.15	5.8	6.36
F5	3.32	3.41	3.53	3.72	3.62	3.73	3.8	4.02
Impact of fault on power grid								
F1	3.6	3.8	4	4.5	3.9	4	4.4	4.8
F2	3.4	3.3	3.4	3.8	3.7	3.6	3.5	4.1
F3	2.6	3	3.3	3.76	3.5	3.6	3.84	3.9
F4	5.19	4.7	4.5	5.12	5.33	5.23	4.85	5.35
F5	3.0	3.2	3.3	3.6	3.4	3.56	3.7	3.8

It becomes evident that application of the reconfiguration method optimizes the overall system performance through increasing peak power with minimization of multiple peaks as given in Table 8.

It is established that CIGS PV material maximizes power generation and gives higher efficiency than crystalline PV. It is pertinent to mention that ocuurance of fault on one PV cell in CIGS PV module does not affect the generated power of the remaining cells of the module. On contrary, the whole PV module working is affected upon any fault occurrence in polycrystalline PV. Thus, CIGS PV yields higher power under faulty conditions.

V. CONCLUSION

In this study, a reconfiguration method is adopted for optimizing the performance of PV array under different fault scenarios. The reconfigured PV array is compared with three different PV interconnection schemes including SP, BL, and TCT. It is found that adoption of RM can increase power generation of a non-uniformly shaded PV array under the considered faults. In addition, a comparison of polycrystalline and CIGS PV materials in terms of power generation is also presented. It is found that CIGS PV material can yield more power output than polycrystalline under the introduced faults with less severe impact on the power grid through an increase in the tracked MPP. The obtained results clearly demonstrate that output power can be increased through reconfiguring of PV modules under developed multiple fault scenarios which is a major contribution of this research, and the adoption of thin film PV material can minimize the power losses with optimized performance of power grid under the studied fault conditions. It is also clearly shown that application of the presented reconfiguration method significantly improves the performance of PV system under all fault scenarios.

ACKNOWLEDGMENT

The publication charges of this paper is paid by the Qatar National Library, Doha, Qatar. The statements made herein are solely the responsibility of the authors.

REFERENCES

[1] M. Sabbaghpur Arani and M. A. Hejazi, "The comprehensive study of electrical faults in PV arrays," *J. Elect. Comput. Eng.*, vol. 2016, Dec. 2016, Art. no. 8712960.

[2] S. K. Firth, K. J. Lomas, and S. J. Rees, "A simple model of PV system performance and its use in fault detection," *Sol. Energy*, vol. 84, no. 4, pp. 624–635, Apr. 2010.

[3] B. A. R. Anderson, *Fundamentals of Semiconductor Devices*. New York, NY, USA: McGraw-Hill, 2004.

[4] C. Lee, J. Suh, and Y. Choi, "Comparative study on module connections to minimize degradation of photovoltaic systems due to bird droppings," *Int. J. Renew. Energy Res.*, vol. 8, no. 1, pp. 230–237, Mar. 2018.

[5] H. Patel and V. Agarwal, "MATLAB-based modeling to study the effects of partial shading on PV array characteristics," *IEEE Trans. Energy Convers.*, vol. 23, no. 1, pp. 302–310, Mar. 2008.

[6] D. Nguyen and B. Lehman, "Modeling and simulation of solar PV arrays under changing illumination conditions," in *Proc. IEEE Workshops Comput. Power Electron.*, Sep. 2006, pp. 295–299.

[7] M. Davarifar, A. Rabhi, and A. E. Hajjaji, "Comprehensive modulation and classification of faults and analysis their effect in DC side of photovoltaic system," *Energy Power Eng.*, vol. 05, no. 04, pp. 230–236, 2013.

[8] M. K. Alam, F. Khan, J. Johnson, and J. Flicker, "A comprehensive review of catastrophic faults in PV arrays: Types, detection, and mitigation techniques," *IEEE J. Photovolt.*, vol. 5, no. 3, pp. 982–997, May 2015.

[9] G. Han, S. Zhang, P. P. Boix, L. H. Wong, L. Sun, and S. Y. Lien, "Towards high efficiency thin film solar cells," *Progr. Mater. Sci. J.*, vol. 87, pp. 246–291, Jun. 2017.

[10] D. A. Quansah and M. S. Adaramola, "Comparative study of performance degradation in poly- and mono-crystalline-Si solar PV modules deployed in different applications," *Int. J. Hydrogen Energy*, vol. 43, no. 6, pp. 3092–3109, Feb. 2018.

[11] V. Bostan, A. R. Toma, T. Tudorache, S. V. Paturca, A.-M. Dumitrescu, and I. Bostan, "Performance analysis of polycrystalline and CIS thin-film PV panels in real operation conditions," in *Proc. 5th Int. Symp. Elect. Electron. Eng. (ISEEE)*, Galati, Romania, Oct. 2017, pp. 1–4.
[12] T. Ozden, B. G. Akinoglu, and S. Kurtz, "Performance and degradation analyses of two different PV modules in central anatolia," in *Proc. Int. Conf. Photovoltaic Sci. Technol. (PVCon)*, Ankara, Turkey, Jul. 2018, pp. 1–4.
[13] A. Kumar, R. K. Pachauri, and Y. K. Chauhan, "Experimental analysis of SP/TCT PV array configurations under partial shading conditions," in *Proc. IEEE 1st Int. Conf. Power Electron., Intell. Control Energy Syst. (ICPEICES)*, Delhi, India, Jul. 2016, pp. 1–6.
[14] A. Mehiri, A.-K. Hamid, and S. Almazrouei, "The effect of shading with different PV array configurations on the grid-connected PV system," in *Proc. Int. Renew. Sustain. Energy Conf. (IRSEC)*, Tangier, Morocco, Dec. 2017, pp. 1–6.
[15] S. R. Pendem and S. Mikkili, "Performance evaluation of series, series-parallel and honey-comb PV array configurations under partial shading conditions," in *Proc. 7th Int. Conf. Power Syst. (ICPS)*, Pune, India, Dec. 2017, pp. 749–754.
[16] B. Veerasamy, T. Takeshita, A. Jote, and T. Mekonnen, "Mismatch loss analysis of PV array configurations under partial shading conditions," in *Proc. 7th Int. Conf. Renew. Energy Res. Appl. (ICRERA)*, Paris, France, Oct. 2018, pp. 1162–1183.
[17] P. R. Satpathy, S. Jena, B. Jena, and R. Sharma, "Comparative study of interconnection schemes of modules in solar PV array network," in *Proc. Int. Conf. Circuit, Power Comput. Technol. (ICCPCT)*, Kollam, India, Apr. 2017, pp. 1–6.
[18] G. Velasco, F. Guinjoan, and R. Pique, "Grid-connected PV systems energy extraction improvement by means of an electric array reconfiguration (EAR) strategy: Operating principle and experimental results," in *Proc. IEEE PESC*, Rhodes, Greece, Jun. 2008, pp. 1983–1988.
[19] R. Candela, V. di Dio, E. R. Sanseverino, and P. Romano, "Reconfiguration techniques of partial shaded PV systems for the maximization of electrical energy production," in *Proc. Int. Conf. Clean Elect. Power*, Capri, Italy, May 2007, pp. 716–719.
[20] B. Dhanalakshmi and N. Rajasekar, "Dominance square based array reconfiguration scheme for power loss reduction in solar PhotoVoltaic (PV) systems," *Energy Convers. Manage.*, vol. 156, pp. 84–102, Jan. 2018.
[21] A. S. Yadav, R. K. Pachauri, Y. K. Chauhan, S. Choudhury, and R. Singh, "Performance enhancement of partially shaded PV array using novel shade dispersion effect on magic-square puzzle configuration," *Sol. Energy*, vol. 144, pp. 780–797, Mar. 2017.
[22] B. Dhanalakshmi and N. Rajasekar, "A novel competence square based PV array reconfiguration technique for solar PV maximum power extraction," *Energy Convers. Manage.*, vol. 174, pp. 897–912, Oct. 2018.
[23] G. Velasco-Quesada, F. Guinjoan-Gispert, R. Pique-Lopez, M. Roman-Lumbreras, and A. Conesa-Roca, "Electrical PV array reconfiguration strategy for energy extraction improvement in grid-connected PV systems," *IEEE Trans. Ind. Electron.*, vol. 56, no. 11, pp. 4319–4331, Nov. 2009.
[24] Y. Liu, Z. Pang, and Z. Cheng, "Research on an adaptive solar photovoltaic array using shading degree model-based reconfiguration algorithm," in *Proc. Chin. Control Decis. Conf.*, May 2010, pp. 2356–2360.
[25] B. Patnaik, J. Mohod, and S. P. Duttagupta, "Dynamic loss comparison between fixed-state and reconfigurable solar photovoltaic array," in *Proc. 38th IEEE Photovoltaic Specialists Conf.*, Jun. 2012, pp. 1633–1638.
[26] M. Karakose and M. Baygin, "Image processing based analysis of moving shadow effects for reconfiguration in PV arrays," in *Proc. IEEE Int. Energy Conf. (ENERGYCON)*, May 2014, pp. 683–687.
[27] B. I. Rani, G. S. Ilango, and C. Nagamani, "Enhanced power generation from PV array under partial shading conditions by shade dispersion using Su Do Ku configuration," *IEEE Trans. Sustain. Energy*, vol. 4, no. 3, pp. 594–601, Jul. 2013.
[28] S. N. Deshkar, S. B. Dhale, J. S. Mukherjee, T. S. Babu, and N. Rajasekar, "Solar PV array reconfiguration under partial shading conditions for maximum power extraction using genetic algorithm," *Renew. Sustain. Energy Rev.*, vol. 43, pp. 102–110, Mar. 2015.
[29] N. A. Rajan, K. D. Shrikant, B. Dhanalakshmi, and N. Rajasekar, "Solar PV array reconfiguration using the concept of standard deviation and genetic algorithm," *Energy Procedia*, vol. 117, pp. 1062–1069, Jun. 2017.
[30] T. Sudhakar Babu, J. Prasanth Ram, T. Dragičević, M. Miyatake, F. Blaabjerg, and N. Rajasekar, "Particle swarm optimization based solar PV array reconfiguration of the maximum power extraction under partial shading conditions," *IEEE Trans. Sustain. Energy*, vol. 9, no. 1, pp. 74–85, Jan. 2018.
[31] S. G. Krishna and T. Moger, "Optimal SuDoKu reconfiguration technique for total-cross-tied PV array to increase power output under non-uniform irradiance," *IEEE Trans. Energy Convers.*, vol. 34, no. 4, pp. 1973–1984, Dec. 2019.
[32] P. R. Satpathy, R. Sharma, and S. Dash, "An efficient SD-PAR technique for maximum power generation from modules of partially shaded PV arrays," *Energy*, vol. 175, pp. 182–194, May 2019.
[33] R. K. Pachauri and Y. K. Chauhan, "Hybrid PV/FC stand alone green power generation: A perspective for Indian rural telecommunication systems," in *Proc. Int. Conf. Issues Challenges Intell. Comput. Techn. (ICICT)*, Ghaziabad, India, Feb. 2014, pp. 7–8.
[34] R. H. G. Tan and L. Y. H. Hoo, "DC-DC converter modeling and simulation using state space approach," in *Proc. IEEE Conf. Energy Convers. (CENCON)*, Johor Bahru, Malaysia, Oct. 2015, pp. 42–47.
[35] J. Ahmed and Z. Salam, "A critical evaluation on maximum power point tracking methods for partial shading in PV systems," *Renew. Sustain. Energy Rev.*, vol. 47, pp. 933–953, Jul. 2015.
[36] P.-Y. Sevilla-Camacho, M.-A. Zuñiga-Reyes, J.-B. Robles-Ocampo, R. Castillo-Palomera, J. Muñiz, and J. Rodríguez-Reséndiz, "A novel fault detection and location method for PV arrays based on frequency analysis," *IEEE Access*, vol. 7, pp. 72050–72061, 2019.
[37] H. López, J. Rodríguez-Reséndiz, X. Guo, N. Vázquez, and R. V. Carrillo-Serrano, "Transformerless common-mode current-source inverter grid-connected for PV applications," *IEEE Access*, vol. 6, pp. 62944–62953, 2018.
[38] R. Dabou, N. Sahouane, A. Necaibia, M. Mostefaoui, F. Bouchafaa, A. Rouabhia, A. Ziane, and A. Bouraiou, "Impact of partial shading and PV array power on the performance of grid connected PV station," in *Proc. 18th Int. Conf. Sci. Techn. Autom. Control Comput. Eng. (STA)*, Monastir, Tunisia, Dec. 2017, pp. 476–481.
[39] X. Sun, T. Silverman, R. Garris, C. Deline, and M. A. Alam, "An illumination-and temperature-dependent analytical model for copper indium gallium diselenide (CIGS) solar cells," *IEEE J. Photovolt.*, vol. 6, no. 5, pp. 1298–1307, Sep. 2016.
[40] T. J. Silverman, "Thermal and electrical effects of partial shade in monolithic thin-film photovoltaic modules," *IEEE J. Photovolt.*, vol. 5, no. 6, pp. 1742–1747, Nov. 2015.
[41] A. Benmir and M. S. Aida, "Analytical modeling and simulation of CIGS solar cells," *Energy Procedia*, vol. 36, pp. 618–627, 2013.
[42] I. U. Khalil, A. Ul-Haq, Y. Mahmoud, M. Jalal, M. Aamir, M. U. Ahsan, and K. Mehmood, "Comparative analysis of photovoltaic faults and performance evaluation of its detection techniques," *IEEE Access*, vol. 8, pp. 26676–26700, 2020, doi: 10.1109/ACCESS.2020.2970531.
[43] J.-M. Huang, R.-J. Wai, and W. Gao, "Newly-designed fault diagnostic method for solar photovoltaic generation system based on IV-curve measurement," *IEEE Access*, vol. 7, pp. 70919–70932, 2019, doi: 10.1109/ACCESS.2019.2919337.

AZHAR UL-HAQ received the Ph.D. degree in electrical engineering from the University of L'Aquila, Italy, and the University of Waterloo, Canada, through the joint Research Doctoral Program. He has been working as an Assistant Professor of electrical engineering with the National University of Sciences and Technology, Islamabad, since October 2016. He worked as a Research Assistant with the Department of ECE, University of Waterloo, Canada, in 2015. His research interests include the grid integration of renewable energies, PV powered smart charging of electric vehicles, and direct load control strategies for peak-shaving in power systems.

RASHID ALAMMARI received the B.S. degree (then got a scholarship) from Qatar University, in 1985, the M.Sc. degree from Washington State University, USA, in 1989, and the Ph.D. degree from Strathclyde University, Glasgow, U.K., in 1996, all in electrical engineering, majoring in power systems. He started as a Teaching Assistant with an industry experience partnership with the Ministry of Electricity and Water. He became an assistant professor, in 1996, and was promoted to an associate professor, in 2003. He was appointed as the Head of the QU Foundation Program, from 1998 to 2000, and then as the Chairman of the Department of Electrical Engineering, from 2000 to 2004, leading the department to its first ABET accreditation. He is a published author of many academic studies on power systems and power quality. He received the University Distinguished Faculty Research Award, in 2004, and achieved the State of Qatar Incentive Award in Electrical Engineering, in 2012. In October 2012, he was appointed as the Dean of the College of Engineering, Qatar University, from October 2012 to March 2016.

ATIF IQBAL (Senior Member, IEEE) received the B.Sc. degree (gold medal) and M.Sc. degrees in engineering (power systems and drives) from Aligarh Muslim University (AMU), Aligarh, India, in 1991 and 1996, respectively, the Ph.D. degree from Liverpool John Moores University, Liverpool, U.K., in 2006, and the D.Sc. (habilitation) degree in control, informatics, and electrical engineering from the Gdansk University of Technology, in 2019. He is a Fellow of the IET, U.K., and the IE, India. He is a Full Professor with the Department of Electrical Engineering, Qatar University, and a Former Full Professor of electrical engineering with Aligarh Muslim University (AMU), Aligarh, India. He was a recipient of the Outstanding Faculty Merit Award, from 2014 to 2015, and research excellence awards Qatar University, Doha, Qatar, in 2015 and 2019. He has been employed as a Lecturer with the Department of Electrical Engineering, AMU, Aligarh, since 1991, where he served as a Full Professor, until August 2016. He was a recipient of Maulana Tufail Ahmad Gold Medal for standing first at the B.Sc.Engg. degree (electrical) exams from AMU, in 1991. He has received several best research paper awards from the IEEE ICIT 2013, IET SEISCON 2013, SIGMA 2018, and the IEEE CENCON 2019. He has published widely in international journals and conferences, and his research findings are related to power electronics, variable speed drives, and renewable energy sources. He has authored or coauthored more than 390 research articles, two books, and three chapters in two other books. He has supervised several large research and development projects worth more than U.S. $8 million. He has supervised and co-supervised several Ph.D. students. His principal areas of research interest are smart grids, complex energy transition, active distribution networks, electric vehicles drivetrain, sustainable development and energy security, and distributed energy generation. He is an Associate Editor of IEEE Access, the Editor-in-Chief of the *Journal of Electrical Engineering* (I'manager), and the Former Associate Editor of the IEEE Transactions on Industry Applications.

MARIUM JALAL received the Ph.D. degree in electrical engineering from L'Aquila, Italy, in April 2015. She was awarded with Gold Medal for the Best M.Sc. Thesis from LCWU, Lahore. From 2011 to 2014, she was a Marie-Curie Early Stage Researcher with the Center of Excellence for Research DEWS, University of L'Aquila, Italy. Her research interests include smart grid technologies and energy efficiency techniques in smart cities. She is a recipient of several research and travel grant awards.

SABA GUL received the B.S. degree in electronic engineering from the Sir Syed University of Engineering and Technology, Pakistan, in 2017, and the M.S. degree in power and control systems from the College of Electrical and Mechanical Engineering, National University of Sciences and Technology (NUST), Islamabad, Pakistan. She has been working as a Research Engineer with NUST. Her research interests include impact of renewable energy integration, and power system stability issues.